Phosphate transport kinetics and structure-function relationships of SLC34 and SLC20 proteins

Forster, Ian C ; Hernando, Nati ; Biber, Jürg ; Murer, Heini

Abstract: Transport of inorganic phosphate (P(i)) is mediated by proteins belonging to two solute carrier families (SLC20 and SLC34). Members of both families transport P(i) using the electrochemical gradient for Na(+). The role of the SLC34 members as essential players in mammalian P(i) homeostasis is well established, whereas that of SLC20 proteins is less well defined. The SLC34 family comprises the following three isoforms that preferentially cotransport divalent P(i) and are expressed in epithelial tissue: the renal NaPi-IIa and NaPi-IIc are responsible for reabsorbing P(i) in the proximal tubule, whereas NaPi-IIb is more ubiquitously expressed, including the small intestine, where it mediates dietary P(i) absorption. The SLC20 family comprises two members (PiT-1, PiT-2) that preferentially cotransport monovalent P(i) and are expressed in epithelial as well as nonepithelial tissue. The transport kinetics of members of both families have been characterized in detail using heterologous expression in Xenopus oocytes. For the electrogenic NaPi-IIa/b, and PiT-1,-2, conventional electrophysiological techniques together with radiotracer methods have been applied, as well as time-resolved fluorometric measurements that allow new insights into local conformational changes of the protein during the cotransport cycle. For the electroneutral NaPi-IIc, conventional tracer uptake and fluorometry have been used to elucidate its transport properties. The 3-D structures of these proteins remain unresolved and structure-function studies have so far concentrated on defining the topology and identifying sites of functional importance.

DOI: https://doi.org/10.1016/B978-0-12-394316-3.00010-7

Current Topics in Membranes-Cotransport Systems

Phosphate transport- *kinetics and structure-function relationships of SLC34 and SLC20 proteins*

Ian C. Forster, Nati Hernando, Jürg Biber and Heini Murer

Institute of Physiology and Zurich Center for Integrative Human Physiology, University of Zurich, Winterthurerstrasse 190,CH-8057 Zurich, Switzerland

Corresponding author: Ian C. Forster PhD
Email: iforster@access.uzh.ch,

Keywords: SLC20, SLC34, phosphate, cotransport, electrogenicity, structure-function

ABBREVIATIONS: ADHR: autosomal-dominant hypophosphatemic rickets; HHRH:hypophosphatemic rickets with hypercalciuria ; MTS: methane thiosulfonate ; PFA: phosphonoformic acid ; PDZ: Post synaptic density protein, Drosophila disc large tumor suppressor, and Zonula occludens-1 protein; PTH: parathyroid hormone; SCAM: substituted cysteine accessibility method ; TEVC: two electrode voltage-clamp; TMD: transmembrane domain ; VCF: voltage-clamp fluorometry

I. OVERVIEW

Transport of inorganic phosphate (P_i) is mediated by proteins belonging to 2 solute carrier families (SLC20 and SLC34). Members of both families transport P_i using the electrochemical gradient for Na^+. Whereas the role of the SLC34 members as essential players in mammalian P_i homeostasis is well established, that of SLC20 proteins is less well defined. The SLC34 family comprises the following 3 isoforms that preferentially cotransport divalent P_i and are expressed in epithelial tissue: the renal NaPi-IIa and NaPi-IIc are responsible for reabsorbing P_i in the proximal tubule, whereas NaPi-IIb is more ubiquitously expressed, including the small intestine, where it mediates dietary P_i absorption. The SLC20 family comprises 2 members (PiT-1, PiT-2) that preferentially cotransport monovalent P_i and are expressed in epithelial as well as non-epithelial tissue. The transport kinetics of members of both families have been characterized in detail using heterologous expression in *Xenopus* oocytes. For the electrogenic NaPi-IIa/b, and PiT-1,-2, conventional electrophysiological techniques together with radiotracer methods have been applied, as well as time-resolved fluorometric measurements that allow new insights into local conformational changes of the protein during the cotransport cycle. For the electroneutral NaPi-IIc, conventional tracer uptake and fluorometry have been used to elucidate its transport properties. The 3-D structures of these proteins remain unresolved and structure-function studies have so far concentrated on defining the topology and identifying sites of functional importance.

II. INTRODUCTION

In mammals, phosphate plays essential structural, metabolic, synthesis and signaling roles. Dietary phosphate is absorbed in the small intestine and circulates in the blood for delivery to soft tissue and bone as required. In plasma, 50% of phosphate is ionized inorganic phosphate (P_i), and the remainder comprises diffusible phosphate complexes (40%) and non-diffusable protein-bound phosphate (10%). In the physiological range of pH, titratable P_i is distributed between monovalent ($H_2PO_4^-$) and divalent (HPO_4^{2-}) ions according to the pH. Under normal conditions, the daily intake of phosphate and loss in feces and urine are balanced and the total plasma P_i lies in the range 0.8-1.5 mM (in humans). The principle locus of P_i homeostasis is the kidney. At the glomerulus, P_i is freely filtered from the blood and then reabsorbed from the primary urine according to the bodily requirements; any excess P_i is excreted in the urine. Approximately 80% of P_i reabsorption occurs along the proximal tubule of the nephron (e.g. (Berndt 1992)) and the remaining 20% is reabsorbed along the distal tubule**.** Proximal tubular P_i reabsorption is under the control of circulating hormones such as parathyroid hormone (PTH), growth hormone, thyroid hormone, the plasma P_i level itself, as well as a number of circulating proteins, collectively referred to as phosphotonins (e.g. (Berndt&Kumar 2007)). The transmembrane flux of anionic P_i (monovalent or divalent) into the cytosol against its electrochemical gradient, requires active transport mechanisms. In mammals, this need is fulfilled by secondary-active carrier proteins that have a high specificity for either $H_2PO_4^-$ or HPO_4^{2-} and use the inwardly directly electrochemical gradient of Na^+ as a free energy source to drive transport.

The two protein families considered in this review are gene products of the SLC20 and SLC34 solute carrier families, designated according to the solute carrier classification established by the Human Genome Organization (Hediger, Romero et al. 2004), www.bioparadigms.org/slc. This nomenclature will be used also when referring to non-

mammalian orthologs. The gene products of the SLC34 family, often referred to as type II Na^+/P_i cotransporters, (or NaPi-II), comprise 3 isoforms: NaPi-IIa, NaPi-IIb and NaPi-IIc (SLC34A1, SLC34A2, SLC34A3, respectively). They are the principal active transport proteins for P_i absorption in the gut and reabsorption in the kidney. Those of the SLC20 family, also known as type III Na^+/P_i cotransporters, are currently represented by 2 isoforms, PiT-1 and PiT-2 (SLC20A1, SLC20A2, respectively). Until recently, they were considered to fulfil a housekeeping role consistent with their ubiquitous expression. However, new evidence suggests they fulfil specific roles in certain organs as outlined below.

Members of a 3rd transporter gene family, SLC17 (Reimer&Edwards 2004) were originally referred to as type I Na^+-dependent P_i transporters because the first cloned member of this family (NaPi-1) was originally shown to be a Na^+-dependent P_i transporter, using the *Xenopus* oocyte expression system (Werner, Moore et al. 1991). This protein was later shown to transport organic anions (Busch, Schuster et al. 1996; Broer, Schuster et al. 1998). Another SLC17 protein, BNP1, was also first classified as a Na^+/P_i transporter, but was then found to mediate vesicular glutamate transport (Bellocchio, Reimer et al. 2000). Thus, given their non-specificity for transporting P_i, SLC17 proteins are no longer considered exclusively Na^+/P_i cotransporters and they will not be considered further in this review.

Finally, it should be noted that the mechanism by which P_i effluxes across the basolateral membrane of epithelial cells still remains unknown, the general concensus being that a yet to be identified anion exchanger is responsible (e.g. (Barac-Nieto, Alfred et al. 2002)).

A. SLC34 family

The SLC34 proteins are the most extensively characterized in terms of their function, structure and regulation. They play vital physiological roles in the kidney for maintaining P_i homeostasis (for review see (Murer, Hernando et al. 2000; Forster, Hernando et al. 2006)).

Transport studies in the pre-cloning era using membrane vesicles from renal and intestinal epithelial tissue documented secondary-active, Na^+-dependent P_i transport ((Berner, Kinne et al. 1976; Hoffmann, Thees et al. 1976)). Further studies used both cloned transporters and native tissue to characterize the kinetics and regulation of this transport (for review see (Murer, Hernando et al. 2000; Biber, Hernando et al. 2009).

Fig 1A compares the phylogeny of representative members of the SLC34 family from different species, including a bacterial ancestor from *V. Cholera* (NptA)). All eukaryotic isoforms are predicted to have the same secondary topology (Fig 1A, *inset*) comprising 12 α-helical units, cytosolic N- and C-termini and a common inverted repeat re-entrant motif. This latter feature is also predicted for NptA (Lebens, Lundquist et al. 2002), and is therefore thought to constitute the transport pathway and be involved in substrate coordination in all SLC34 proteins (Werner&Kinne 2001). An important mechanistic sub-classification of SLC34 family gene products concerns their electrogenicity. SLC34A1 and SLC34A22 (NaPi-IIa/b) are electrogenic, whereas SLC34A3 (NaPi-IIc) is electroneutral (Fig 1A).

Fig 1 near here

The first family member (SLC34A1or NaPi-IIa) was identified by expression cloning using *Xenopus* oocytes and a cDNA library derived from rat and human kidney (Magagnin, Werner et al. 1993). Immunohistochemistry confirmed its localization at the apical membrane of renal proximal tubular cells. NaPi-IIa has since been detected in other tissues such as brain, osteoclasts and osteoblast-like cells (Lundquist, Murer et al. 2007) that suggests a potentially wider expression profile for this “renal” isoform. Nevertheless the relative mRNA distribution for NaPi-IIa in humans is clearly weighted in favour of the kidney (Nishimura&Naito 2008). Following the cloning of several NaPi-IIa isoforms, a Na^+-P_i cotransporter from the kidney and intestine of winter flounder was identified (Werner, Murer et al. 1994; Kohl, Herter et al. 1996). Its mammalian cousin (SLC34A2 or NaPi-IIb) was then cloned using a mouse

embryonic EST clone (Hilfiker, Hattenhauer et al. 1998) and localized to the brush border membrane of enterocytes and a number of other organs and tissues, including lung, colon, testes, salivary gland, thyroid gland mammary gland, uterus and liver (Hilfiker, Hattenhauer et al. 1998; Frei, Gao et al. 2005; Nishimura&Naito 2008). In contrast to the flounder NaPi-IIb isoform, which is expressed in both kidney and intestine (Kohl, Herter et al. 1996), mammalian NaPi-IIb does not appear to be expressed at the protein level in the kidney. At the primary amino acid sequence level, NaPi-IIb isoforms are distinguished from the renal NaPi-IIa by a unique clustering of cysteine residues in their C-terminal region.

The 3rd member of the SLC34 family to be identified (SLC34A3 or NaPi-IIc), like NaPi-IIa, is considered a renal-specific P_i transporter and is also apically expressed in the renal proximal tubule (Segawa, Kaneko et al. 2002; Madjdpour, Bacic et al. 2004; Picard, Capuano et al. 2010). It is distinguished from the other SLC34 proteins by its high expression in weaning animals, a cysteine cluster in the C-terminal region like NaPi-IIb, and the distinctive functional hallmark of electroneutrality (Segawa, Kaneko et al. 2002).

In other respects, all 3 SLC34 members show a molecular identity of about 75% {Bacconi, 2005 #334}, if the N- and C- termini and the prominent extracellular loop that separates the protein into two halves are excluded (see IV, Structure- Function Relationships).

The expression and regulation of SLC34 proteins in their intestinal and renal context has been studied extensively because these organs represent the principle entry and exit points respectively for P_i in mammals. Renal regulation of NaPi-IIa has been the subject of extensive reviews (Murer, Hernando et al. 2000; Werner&Kinne 2001; Tenenhouse&Murer 2003; Miyamoto, Segawa et al. 2004; Tenenhouse 2005; Forster, Hernando et al. 2006). The regulation of P_i reabsorption centers on controlling the number of transporter proteins in the proximal tubule brush border membrane. So far there is no evidence to suggest that the transport kinetics themselves are the target of regulatory factors.

The importance of SLC34 proteins in mammalian P_i handling is underscored by knockout animal studies and identification of naturally occurring mutations in patients with specific symptoms associated with impaired P_i homeostasis (for review see (Miyamoto, Haito-Sugino et al. 2011)). The critical role of NaPi-IIa for P_i homeostasis is further evidenced by the hyperphosphaturia phenotype documented in NaPi-IIa knockout mouse ($Npt2a^{-/-}$) (Beck, Karaplis et al. 1998). Dysregulation of NaPi-IIa abundance causes P_i-deficiency disorders, such as X-linked hypophosphatemia (XLH) and autosomal-dominant hypophosphatemic rickets (ADHR) (reviewed in (Tenenhouse 2005)). No mutation in the NaPi-IIa gene has yet to be unequivocally linked to human hypophosphotemic disorders, and the present consensus is that the mutations alone are not responsible for the clinical disorders in the patients (Tenenhouse&Murer 2003). On the other hand, naturally occurring mutations in the NaPi-IIc gene have been linked to the rare P_i-handling disease hereditary hypophosphatemic rickets with hypercalcuria (HHRH) (Bergwitz, Roslin et al. 2006; Lorenz-Depiereux, Benet-Pages et al. 2006). Mutations in the NaPi-IIb gene have been proposed to cause pulmonary alveolar microlithiasis and possibly linked to testicular microlithiasis (Corut, Senyigit et al. 2006). In general, these mutations result in truncations and mistargeting to the plasma membrane rather than altered transport function of the protein itself.

B. SLC20 family

SLC20 proteins show a widespread expression based primarily on the detection of mRNA in both epithelial and non-epithelial tissue (Tatsumi, Segawa et al. 1998; Uckert, Willimsky et al. 1998; Bai, Collins et al. 2000; Nishimura&Naito 2008). Consequently, it was proposed that they fulfil a “housekeeping” role for P_i entry into most cells. They are represented by the two isoforms SLC20A1 (PiT-1) and SLC20A2 (PiT-2) that were originally identified as retroviral receptors that allow viral entry following a specific interaction with the receptor (Collins, Bai et al. 2004). That the retroviral receptor Glvr-1, which renders cells

susceptible to infection by the gibbon ape leukemia virus, was also a P_i transporter was first proposed from its close homology to a phosphate permease (PHO-4) from the fungi *Neurospora crassa* (Johann, Gibbons et al. 1992). A related protein, which renders cells susceptible to infection by amphotropic murine retrovirus (Ram-1) was subsequently identified (Miller&Miller 1994; van Zeijl, Johann et al. 1994). Experimental evidence showing that retroviral receptors Glvr-1 and Ram-1 are electrogenic Na^+-dependent cotransporters then followed (Kavanaugh, Miller et al. 1994; Olah, Lehel et al. 1994; Kavanaugh&Kabat 1996), and the receptors were thereafter renamed PiT-1 and PiT-2, respectively.

Proteins related to PiT-1 and PiT-2 are present in all phyla (Fig 1B). However, one distinguishing feature concerns the driving cation. In prokaryotes and plants, P_i transport mediated by these proteins is coupled to the H^+ gradient (van Veen 1997; Daram, Brunner et al. 1999; Harris, Webb et al. 2001), whereas in animals and fungi, transport is coupled to the Na^+ gradient (Versaw&Metzenberg 1995; Martinez&Persson 1998; Tatsumi, Segawa et al. 1998; Uckert, Willimsky et al. 1998; Bai, Collins et al. 2000). SLC20 proteins are presumed to have the same secondary structure (Fig1B, *inset*) with a common inverted repeat topology that differs significantly from that of SLC34 proteins. Moreover, it is assumed that SLC20 proteins are all electrogenic based on functional studies. Recent evidence also indicates that in addition to their housekeeping role, SLC20 proteins perform important physiological roles in bone P_i metabolism and in pathological conditions, such as hyperphosphatemia-induced calcification of vascular tissue (e.g. (Ketteler&Giachelli 2006)), osteoarthritis (Cecil, Rose et al. 2005). Importantly, PiT-2 could play a significant role in dietary regulated P_i transport in the kidney, alongside NaPi-IIa and NaPi-IIc (Moe 2009; Villa-Bellosta, Ravera et al. 2009). The expression of both SLC20 isoforms at the mRNA level in human tissue confirms their ubiquity (Nishimura&Naito 2008). Like SLC34 proteins, recent studies have further

highlighted their developmental and physiological importance, pointing to novel and specific roles for this family. For example, loss of function mutations in the PiT-2 gene were reported that are implicated in disturbed brain P_i homeostasis (familial idiopathic basal ganglia calcification) (Wang, Li et al. 2012). Furthermore, a PiT-1-/- mouse was reported to be embryonic fatal, which suggested a critical role for PiT-1 in liver development (Beck, Leroy et al. 2010).

This review focuses on the transport mechanism and structure-function relationships of SLC34 and SLC20 proteins. Given that it is the number of transporters in the membrane that determines the P_i flux, the characterization of the transport mechanisms and kinetic properties of these proteins is crucial to define the P_i flux contribution of a mixed population of transporters. Furthermore, the structure-function relationships can lead to greater insight into developing pharmaceuticals to target specific transporters. At the molecular level, 3-D crystal structures of SLC34 and SLC20 family members or their bacterial homologs are unavailable and therefore indirect methods (biophysical and biochemical) are the only means to correlate function with structure. Our current knowledge of transport mechanism and structure-function relationships has benefitted substantially from expression cloning of the different isoforms to allow investigation by heterologous expression, principally in *Xenopus* oocytes. Moreover, studies on the electrogenic isoforms can employ electrophysiology-based assays that allow resolution of the properties of the transport cycle in real-time. We shall first review the proteins' kinetic properties, based primarily on investigation of the wild-type (WT) and engineered mutants expressed in *Xenopus* oocytes, and then consider their structure-function properties. For more detailed information on the roles SLC34 and SLC20 proteins play in other aspects of P_i handling current, the reader should consult extensive reviews on the physiological roles, regulation and pathophysiological implications (e.g. (Tenenhouse 2005;

Biber, Hernando et al. 2009; Forster, Hernando et al. 2011; Miyamoto, Haito-Sugino et al. 2011)).

III. TRANSPORT KINETICS

A. Steady-state transport properties

An overview of the steady-state properties of the two families is given in the Table.

1. *SLC34*

a. Driving forces. All SLC34 proteins use the inwardly directed Na^+ gradient to catalyze P_i transport (Fig 2A). In addition, under voltage clamp conditions, *Xenopus* oocytes that express the electrogenic isoforms show a strong dependence of P_i-induced current (I_{P_i}) on membrane potential. Typically, a change membrane of potential from 0 mV to-100 mV doubles I_{P_i} (Fig 2A). Based on the finding of a 1:1 correlation between ^{32}P uptake and net charge translocated, I_{P_i} can then be used as a direct measure of the P_i transport rate (Forster, Loo et al. 1999; Virkki, Forster et al. 2005). For most isoforms, the voltage dependence of I_{P_i} also tends to saturate at the extremes of membrane potential, which indicates the existence of rate limiting, voltage-independent partial reactions in the transport cycle (see Section III.B.1). In contrast, no I_{P_i} is detected for NaPi-IIc (Segawa, Kaneko et al. 2002; Bacconi, Virkki et al. 2005). Moreover, ^{32}P uptake rates are independent of membrane potential (Bacconi, Virkki et al. 2005; Ghezzi, Murer et al. 2009) and cation interactions in the absence of P_i show no sensitivity to membrane potential (Ghezzi, Murer et al. 2009).

Fig 2 near here

b. Substrates. All SLC34 isoforms display Michaelian transport kinetics with respect to P_i (by radiotracer uptake or, where possible, by voltage-clamp assays), consistent with the translocation of one P_i molecule per transport cycle (e.g. (Busch, Waldegger et al. 1994; Forster, Wagner et al. 1997; Forster, Hernando et al. 1998; Nalbant, Boehmer et al. 1999;

Segawa, Kaneko et al. 2002; Graham, Nalbant et al. 2003; Virkki, Forster et al. 2005; Forster, Virkki et al. 2006; Ghezzi, Murer et al. 2009)). The apparent affinity constants for total P_i ($K_{0.5}^{Pi}$) are typically <100 μM (pH 7.4 and $[Na^+]$ =100 mM), with the exception of (i) a zebra fish isoform (NaPi-IIb1) ($K_{0.5}^{Pi}$ =250 μM) (Graham, Nalbant et al. 2003), and (ii) the murine and rat NaPi-IIb that exhibit exceptionally high apparent P_i affinities ($K_{0.5}^{Pi}$ ≈10 μM) (Forster, Virkki et al. 2006; Villa-Bellosta&Sorribas 2008). Furthermore, all SLC34 proteins preferentially transport divalent P_i (HPO_4^{2-}) (Forster, Loo et al. 1999; Bacconi, Virkki et al. 2005). For the electrogenic NaPi-IIa and NaPi-IIb, preference for HPO_4^{2-} was established by simultaneously measuring the ratio of net charge translocated to P_i influx using ^{32}P as a tracer, on single voltage clamped oocytes (Forster, Loo et al. 1999). This preference has also been confirmed by surface pH measurements on *Xenopus* oocytes using a pH-sensitive electrode (Ravera, Virkki et al. 2007). For the electroneutral NaPi-IIc, the preference for HPO_4^{2-} is consistent with its 2:1 Na^+:P_i stoichiometry (Bacconi, Virkki et al. 2005) and based on recent surface pH measurements using an ion-sensitive field effect transistor (ISFET) sensor (Schaffhauser, Patti et al. 2012).

With Na^+ as the variable substrate, the cotransport rate (by uptake or voltage clamp) shows sigmoidicity, with reported Hill coefficients ranging from 1.8 (Forster, Loo et al. 1999) to 3 (Forster, Hernando et al. 1998). A Hill coefficient >1 indicates that >1 Na^+ ion is required to drive P_i transport and non-integer values reflect the degree of cooperativity of multiple cation interactions (e.g. (Weiss 1997)). The apparent affinities for Na ($K_{0.5}^{Na}$) are also reasonably consistent among isoforms, lying typically in the range 40-60 mM. The apparent affinities for Na and P_i indicate that under normal mammalian physiological conditions most SLC34 isoforms function at or near their maximum transport velocities.

Inorganic arsenate (As^V), with a similar structure to P_i, is also a potential substrate for SLC34 proteins. Arsenate is known to compete with P_i with an inhibition constant (K_i^{As})

typically ≈1 mM for NaPi-IIa/c but as low as ≈50 μM for NaPi-IIb (Villa-Bellosta&Sorribas 2008), which is consistent with the higher P_i apparent affinity for this isoform. Given that the apparent affinity for As^V is close to K_i^{As} it was therefore proposed that NaPi-IIb could play a significant role in the toxicokinetics of arsenic exposure (Villa-Bellosta&Sorribas 2009; Villa-Bellosta&Sorribas 2010; Beene, Halluer et al. 2011).

c. Stoichiometry and concentrating capacity. Simultaneous voltage-clamp measurement of net charge translocation and uptake (^{32}P or ^{22}Na) was used to resolve previous uncertainties concerning the stoichiometry of electrogenic Na-coupled P_i transport. For rat NaPi-IIa and flounder NaPi-IIb, a consistent value of $3Na:1P_i$ was obtained (Forster, Loo et al. 1999) with one net positive charge translocated per transport cycle. For NaPi-IIc, the predicted stoichiometry of 2:1 was established by dual tracer (^{32}P and ^{22}Na) assay (Bacconi, Virkki et al. 2005). The stoichiometry difference between NaPi-IIa/b and NaPi-IIc means that the theoretical P_i concentrating capacity, assuming a 10:1 Na concentration gradient at a membrane potential of -60 m, is approximately 100-fold higher for NaPi-IIa/b. With a 10-fold greater inward flux of Na^+ ions and net charge movement, compared to NaPi-IIc this would significantly increase the energetic cost to a cell.

d. Cation specificity and pH. Consistent with results from pre-cloning studies on vesicles from native tissue, SLC34 proteins were considered exclusively Na^+-driven as little or no transport activity is observed when other cations fully replace external Na^+. However, it was recently shown that Li^+ ions are able to substitute for at least one of the 3 Na^+ ions in the transport cycle. Moreover, simultaneous electrophysiology and ^{22}Na uptake assays indicate that one Li^+ ion, together with 2 Na^+ions are transported per cycle (Andrini, Meinild et al. 2012). Unlike some other solute carriers, protons do not substitute for Na^+ as the driving cation (Forster, Biber et al. 2000). However, the transport rate of all SLC34 proteins is strongly dependent on pH. Special care must be taken when assessing the effect of pH on

SLC34 transport kinetics because P_i is titratable. Thus, if we assume a pK_a=6.8 for P_i titration in low ionic strength physiological solutions, at pH 7.4, $HPO_4^{2-}/H_2PO_4^-$ =4 and this ratio will be <1 for pH<6.8. In addition, protons alter the transport kinetics by interacting with voltage sensitive partial reactions and competing for the 3rd Na^+ binding interaction (Forster, Biber et al. 2000). The net result is a progressive reduction in maximum transport rate as external [H^+] increases, together with a reduced apparent affinity for HPO_4^{2-}. At low pH (≈5), where P_i is almost only monovalent, P_i can still interact with the protein to block the uncoupled leak current (Ehnes, Forster et al. 2004) (see II.IA.1.f).

e. Binding order. Early steady-state kinetic studies using native tissue established that Na-coupled P_i cotransport proceeds in an ordered manner with Na^+ binding first (e.g. (Hoffmann, Thees et al. 1976)). Studies on NaPi-IIa expressed in *Xenopus* oocytes refined this model by proposing that 1 Na^+ ion interacts with the protein before P_i binds (Forster, Hernando et al. 1998; Forster 2007), consistent with the finding that the Na^+-dependence of the uncoupled leak (see below) showed Michaelian kinetics (Forster, Hernando et al. 1998). Moreover, with saturating P_i, the transport rate is strongly Na^+ -dependent, which indicates that Na^+ is the last substrate to bind before translocation. The proposed "Na-P_i-Na-Na" model (Forster, Hernando et al. 1998) has since been further revised to become the "Na-Na-Pi-Na" model based on (i) evidence from voltage clamp fluorometry studies on NaPi-IIb with an engineered fluorophore labeling site (Virkki, Murer et al. 2006) (section IV.A.3), and (ii) detailed analysis of the wild-type (WT) presteady-state kinetics (e.g (Andrini, Meinild et al. 2012)) (section III.B.2). According to this model, 2 Na^+ ions bind sequentially followed by P_i binding. Finally, a 3rd Na^+ binds before a proposed rate-limiting reorientation of the fully loaded carrier (Fig 2A). Li^+ ions can compete with Na^+ for occupancy of the 1st cation binding site (Andrini, Meinild et al. 2012) (Fig 2A). The order of release of substrates to the cytosol is still unknown.

For the electroneutral NaPi-IIc, evidence from fluorometric assays suggests that, like its electrogenic cousins, 3 Na^+ ions interact but only 2 are translocated and ultimately released to the cytosol to complete the transport cycle (Ghezzi, Murer et al. 2009) (Fig 2A). The fate of 1st bound Na^+ ion is critical in defining the electrogenic properties of the particular isoform: for NaPi-IIa/b, this binds within the transmembrane field and is translocated; for NaPi-IIc, it may simply serve to increase the cooperativity of the 2nd Na^+ interaction before P_i binding (Ghezzi, Murer et al. 2009).

f. Uncoupled leak: Like many cation-coupled cotransporters, electrogenic SLC34 proteins exhibit an uncoupled leak current in the absence of the driven substrate (Forster, Hernando et al. 1998; Andrini, Ghezzi et al. 2008). No evidence for a Na^+-leak is found for the electroneutral NaPi-IIc (Bacconi, Virkki et al. 2005), although naturally occurring mutations in NaPi-IIc have been reported to result in a significant Na^+-leak (Jaureguiberry, Carpenter et al. 2008). The underlying mechanism at the molecular level has yet to be elucidated. Strong experimental evidence supports the notion that the leak observed in WT NaPi-IIa and NaPi-IIb is intrinsic to the protein (Forster, Hernando et al. 1998; Andrini, Ghezzi et al. 2008). The leak current is inhibited by phosphonoformic acid (PFA) (see III.A.3) but, unlike the cotransport activity, the leak is unaffected by external protons. Indeed, the inhibitory action of PFA on the leak current can be recapitulated using P_i at very low pH, where cotransport is fully suppressed (Ehnes, Forster et al. 2004). This salient finding implies that monovalent P_i do interact with SLC34 proteins. Based on the leak current kinetics, it was proposed that the leak results from the movement of the 1st Na^+ ion through the protein in a uniport-like manner (Forster, Hernando et al. 1998; Andrini, Ghezzi et al. 2008) (see Fig 4A). This conclusion is also consistent with the high temperature dependence of the leak current (Bacconi, Ravera et al. 2007). In summary, the leak and cotransport modes are most likely intrinsically related and share the same partial reactions. Under normal physiological

conditions with saturating P_i levels, the leak mode will make a negligible contribution to net Na^+ influx.

g. *Turnover rate*. Transporter turnover rate defines the transport rate of a single protein. This can be determined from a measurement of the transport rate of a population of proteins under defined conditions (e.g. saturating substrate) if the number of active transporters is known. For electrogenic transporters, the steady-state substrate-induced current at a given voltage (V) and substrate concentration for N active transporters is given by:

$$I_S(V) = N\phi(V)\, n_t\, e \qquad 1$$

where $\phi(V)$ is the turnover rate (transport cycles s^{-1}), n_t is the number of charges translocated per cycle and e is the electronic charge. One approach to estimate N uses the ratio of the total mobile charge (Q_{max}) to the apparent valence of each cotransporter functional unit (z) obtained from presteady-state analysis (section III.B.2). The turnover rate is then:

$$\phi(V) = I_S(V) z / (n_t Q_{max}) \qquad 2$$

Published estimates of $\phi(V)$ for SLC34 proteins lie in the range 4-13 s^{-1} (-60 mV, ~20 ^oC) (Forster, Virkki et al. 2006). This range encompasses that reported for other electrogenic cotransporters and is typically <100 s^{-1} (e.g. SGLT-1: 57 s^{-1} (Loo, Hazama et al. 1993); GAT-1: 6 - 15 s^{-1} (Mager, Naeve et al. 1993; Gonzales, Lee et al. 2007); EAAT2: 29 s^{-1} (Wadiche, Arriza et al. 1995); NIS: 36 s^{-1} (Eskandari, Loo et al. 1997). There are strong indications, based on freeze fracture studies of oocyte membranes, that z obtained from presteady-state data is an underestimate of the true charge/carrier (see (Zampighi, Kreman et al. 1995) (Gonzales, Lee et al. 2007)). Therefore, turnover rates using this approach may also be underestimated. Furthermore, SLC34 protein transport kinetics are strongly temperature dependent (e.g. (Bacconi, Ravera et al. 2007)). Thus, we would expect higher values under mammalian physiological conditions (37 ^oC), given that the estimates of ϕ were obtained from oocyte data (18-20 ^oC). If we assume that the temperature dependence of P_i-transport for the

flounder NaPi-IIb (Bacconi, Ravera et al. 2007) is representative for all isoforms (Q_{10}=2.3), then the turnover estimated experimentally for rat NaPi-IIa (4.1 ± 0.6 s^{-1}, at -60 mV) (Forster, Virkki et al. 2006) would be > 10 s^{-1} at 37 ^{o}C. The turnover rate for NaPi-IIc has not been experimentally determined.

2. SLC20

a. *Driving forces*. SLC20 proteins also use the inwardly directed Na^+ gradient to catalyse P_i transport (Fig 2B). From voltage-clamp studies, *Xenopus* oocytes expressing PiT-1 or PiT-2 display a curvilinear dependence of transport rate (P_i-induced current, I_{P_i}) on membrane potential. Typically, a change membrane potential from 0 mV to-100 mV doubles the transport rate (Fig 2B). However, unlike most SLC34 isoforms, evidence for rate limiting behavior at the hyperpolarizing extreme is less apparent (Kavanaugh&Kabat 1996; Ravera, Virkki et al. 2007).

b. *Substrates*. Like SLC34 proteins, SLC20 proteins show Michaelian kinetics with respect to P_i, (by uptake or electrophysiology), consistent with the translocation of one P_i molecule per transport cycle (e.g. (Kavanaugh, Miller et al. 1994; Bai, Collins et al. 2000; Bottger, Hede et al. 2006; Ravera, Virkki et al. 2007)). A cooperative P_i-dependence was reported for PiT-2 expressed in *Xenopus* oocytes under non-voltage clamped conditions, a finding consistent with this isoform behaving as a functional dimer (Bottger, Hede et al. 2006). This finding has yet to be confirmed under voltage-clamp conditions. SLC20 proteins show an apparent affinity constant for total P_i ($K_{0.5}^{Pi}$) typically <100 μM (pH 7.4, [Na^+] =100 mM) and they preferentially transport monovalent P_i ($H_2PO_4^-$) (Saliba, Martin et al. 2006; Ravera, Virkki et al. 2007). The P_i species preference was established by combining electrophysiology and tracer flux assays as for the SLC34 isoforms (Ravera, Virkki et al. 2007), and has also been confirmed by surface pH measurements on *Xenopus* oocytes

(Ravera, Virkki et al. 2007; Schaffhauser, Patti et al. 2012). The preference for monovalent P_i and relative insensitivity of transport kinetics to reduced pH means that SLC20 proteins could support P_i transport under acidotic conditions, where SLC34 proteins are functionally compromised. With Na as the variable substrate, the P_i activation kinetics for PiT1 and PiT2, determined electrophysiologically show no sigmoidicity. Given that the determined stoichiometry is 2:1, this indicates a weak cooperativity between Na interactions. However, for the malarial homolog (PfPIT) a strong cooperativity for Na was found (Saliba, Martin et al. 2006).

As with SLC34 proteins, inorganic arsenate (As^V) was also found to interact with PiT-1 (with $K_{0.5}^{As}$= 0.83 mM), but not for PiT-2 (Ravera, Virkki et al. 2007), however direct evidence for As^V as a cotransported species was lacking in that study. Recently, uptake assays using $^{73}As^V$ as a radiotracer (Villa-Bellosta&Sorribas 2010) established that As^V is indeed transported by both SLC20 isoforms. The somewhat higher $K_{0.5}^{As} \approx 4$ mM may reflect the lack of controlled membrane potential in that study. It is unlikely that SLC20 proteins would provide a significant pathway for arsenic toxification in mammals given the relatively poor apparent affinity for As^V.

c. *Stoichiometry and concentrating capacity*. The Na^+:P_i stoichiometry for PiT-1 of 2:1 has been determined by simultaneous ^{22}Na and ^{32}P uptake under voltage-clamp conditions (Ravera, Virkki et al. 2007) as well as by means of a static-head approach using malarial parasites expressing PfPiT (Saliba, Martin et al. 2006). These findings are consistent with the SLC20 preference for monovalent P_i.

d. *Cation specificity and pH.* PiT-1 is significantly less sensitive to pH compared to the mammalian NaPi-IIa and flounder NaPi-IIb. The maximum transport rate is relatively constant over 3 pH units and $K_{0.5}^{Pi}$ increases significantly only at pH <6. Unlike SLC34 proteins that are exclusively Na^+ driven, for PiT-1, Li^+ can fully replace Na^+ as the driving

cation, albeit with a significantly reduced transport rate (Ravera, Virkki et al. 2007). In the absence of Na^+, lowering pH from 7.5 to 6.0 induced significant P_i uptake in *Xenopus* oocytes that expressed PiT-2. This finding suggests that H^+ may also substitute for Na^+ for this isoform (Bottger, Hede et al. 2006; Villa-Bellosta, Bogaert et al. 2007). The increased $K_{0.5}^{Pi}$ for PiT-1 with acidification suggests that protons may interact directly with the protein to reduce substrate affinity.

e. *Binding order*. Interpretation of assays under voltage clamp conditions with varying substrates suggest that Na^+ is the first ion to interact followed by an apparent random binding of Na^+ and P_i (Ravera, Virkki et al. 2007).

3. *Inhibitors for SLC34 and SLC20 proteins*

a. *SLC34*. Interest in inhibitors focuses on blockers for NaPi-IIb as a means to reduce intestinal P_i absorption in chronic kidney disease. Cotransport by all SLC34 isoforms is inhibited by phosphonoformic acid or foscarnet (PFA) (Loghman-Adham 1996), which competes for P_i binding. However, PFA has a higher K_i (~0.4-0.6 mM (e.g.(Villa-Bellosta&Sorribas 2009)) than $K_{0.5}^{Pi}$ and displays nephrotoxic effects (Loghman-Adham 1996). These characteristics make it unattractive as a means to limit dietary P_i absorption and prevent hyperphosphatemia in cases where kidney function is compromised (Wallin&Ryrfeldt 1995). Other pharmacologically interesting compounds with significantly lower K_i 's compared with PFA have been the subject of commercial studies (Weinstock 2004). These possibly act in a non-competitive manner on SLC34 proteins, as reported for the compound JTP-59557 (Matsuo, Negoro et al. 2005).

b. *SLC20*. PFA is a very poor inhibitor of SLC20-mediated transport activity (Ravera, Virkki et al. 2007; Villa-Bellosta 2007; Villa-Bellosta&Sorribas 2009), and currently no other specific non-transportable inhibitors have been reported.

B. Presteady-state kinetics and voltage dependence

1. ***Background***

The voltage dependence of electrogenic cotransport is postulated to arise from transitions between conformational states that involve charges sensing the membrane potential. At extreme membrane potentials, these partial reactions in the cotransport cycle are no longer rate determining, thereby giving rise to the saturating effects seen in the steady-state I_{P_i} vs V relation (*right panel*, Fig 2A). The charge movements reflect voltage-dependent conformational rearrangements that involve (i) charges intrinsic to the protein (i.e., associated with the empty carrier), and (ii) the movement of external cations to and from their respective binding sites within the protein. For cotransporters, the first experimental evidence for the existence of mobile charges was documented by applying rapid steps in membrane potential to *Xenopus* oocytes heterologously expressing SGLT1 (Loo, Hazama et al. 1993) and GAT1 (Mager, Naeve et al. 1993). With this approach, the time-dependent redistribution of mobile charges from a population of independently functioning transporters manifests itself macroscopically as transient decaying currents, termed presteady-state relaxations. For a single protein, these charge movements would most likely be discrete "shots" of current occurring with the change of conformational state- the probability distribution of which would follow Poisson statistics. They would be well below the detection limit of current instrumentation[1], however a large population of proteins (typically $>10^9$ in the oocyte membrane) gives resolvable decaying currents comprising one or more exponential decays, depending on the number of partial reactions involved.

2. ***SLC34***

a. Basic properties. Presteady-state relaxations attributed to rat/human NaPi-IIa (Forster, Hernando et al. 1998; Virkki, Forster et al. 2005) and flounder/mouse NaPi-IIb (Forster, Wagner et al. 1997; Forster, Virkki et al. 2006; Andrini, Meinild et al. 2012) give a macroscopic view of their molecular-scale movements in real time and have been

instrumental in elucidating the underlying mechanism of the voltage-dependency of SLC34 proteins. The relaxations depend on the external [Na^+], are suppressed by P_i and the inhibitor PFA and are still detectable in the absence of external Na^+ (choline replacement) (Fig 3A). Importantly, the amount of charge displaced for equal but opposite voltage steps is balanced, which confirms that they are capacitative in nature and arise from the displacement of a fixed number of mobile charges within the transmembrane electric field. Presteady-state relaxations are not detectable in *Xenopus* oocytes expressing functional NaPi-IIc, consistent with the notion that no voltage-dependent partial reactions contribute to its transport cycle.

Fig 3 near here

b: Analysis and interpretation. The oocyte endogenous capacitive charging component is first eliminated from the total current (e.g. by curve fitting, or by subtracting the data set obtained with PFA to suppress relaxations), and then the relaxations are fit with a decaying exponential function. The relaxation time constant (τ) plotted as a function of the test (or "target") potential shows strong voltage dependence, as expected for a non-linear dielectric. The characteristic depolarizing shift of the maximum τ with increasing [Na^+] (Fig 3B) indicates that [Na^+] determines that rate of charge movement. Numerical integration of the relaxations gives the charge displaced (Q) as a function of V. For the WT NaPi-IIa/b this relationship shows saturation at the potential extremes, as expected for a discrete number of mobile charges that move within the transmembrane electric field (Fig 3B). The Q-V data can be parameterized by fitting with a single Boltzmann function of the form:

$$Q(V) = Q_{max} / (1 + \exp (V_{0.5} - V)ze/kT) + Q_{hyp} \qquad 3$$

where $Q(V)$ is the charge moved for a voltage step from a given holding potential to V; z is a slope factor (interpreted as the apparent valency, associated with a lumped hypothetical charged entity that moves across the whole transmembrane electric field); Q_{max} is the total displaceable charge; Q_{hyp} is the charge at the hyperpolarizing extreme that depends on the

holding or starting potential;$V_{0.5}$ is the voltage at 50% of the total charge has been displaced; *e* the electronic charge; *k,* Boltzmann's constant and *T* is the absolute temperature. If the charge distribution is first offset by Q_{hyp} and normalized to Q_{max} in maximum [Na^+], a depolarizing shift with increasing [Na^+] is found. This is similar to the shift observed for the τ-*V* data (Fig 3B). The intrinsic mobile charge of the protein (measured in the absence of external Na^+) accounts for ≈40% of the total detected with Na^+ present. A simple kinetic scheme that satisfactorily accounts for these data has 4 states corresponding to 4 conformations of the protein (Andrini, Meinild et al. 2012) (Fig 3C). The empty carrier is assumed to occupy one of 2 states (state 0 or state 1) depending on the membrane potential. For a strong hyperpolarizing change in membrane potential, the protein assumes the "outward" facing conformation (state 1); 2 Na^+ ions can then interact sequentially so that the system occupies state 3 with 2 Na^+ ions bound (Andrini, Meinild et al. 2012).

The dependence on external [Na^+] of the fit parameters (Q_{max}, $V_{0.5}$, *z*) (Eqn 3) reveals important properties that have been used for testing the validity of models for cation interaction. In particular, when the $V_{0.5}$ vs [Na^+] data for the WT flounder NaPi-IIb are plotted semi-logarithmically, a linear relationship for [Na^+]> 25 mM was found with a limiting slope close to ≈120 mV/ decade consistent with the sequential interaction of 2 Na^+ ions (Fig 4B) (Andrini, Meinild et al. 2012)). In contrast, when Li^+ replaced Na^+ in the external medium, the slope with respect to [Li^+] was reduced to ≈60 mV/decade, consistent with one Li^+ ion interacting with the protein (Andrini, Meinild et al. 2012). Deviations from linearity are seen at low [Na^+] where the *Q-V* data can no longer be described in terms of a single Boltzmann function.

c. *A 10 state kinetic model for electrogenic SLC34.* A 10-state kinetic model that describes the electrogenic SLC34 cotransport cycle as a sequence of partial reactions between 10 hypothetical conformational states of the protein has been proposed (Fig 4A). Numerical

simulations using this model predict the steady-state cotransport current (Fig 4B) and presteady-state parameters (Fig 4C) that match closely with those obtained from experimental data, thereby validating its application. In addition to providing basic mechanistic insight into the differences in voltage-dependent kinetics for WT isoforms (e.g., (Forster, Virkki et al. 2006)), and a mechanistic basis for cation interactions (Forster, Biber et al. 2000; Andrini, Meinild et al. 2012), such a model can be used to identify critical partial reactions when the steady-state and presteady-state kinetics are altered by mutagenesis (see Section IV.A.4) (Ehnes, Forster et al. 2004; Bacconi, Ravera et al. 2007; Ghezzi, Murer et al. 2009). At present, the model is severely underdetermined because the kinetics of substrate interaction on the cytosolic side are unknown.

Fig 4 near here

3 *SLC2*.

Oocytes expressing PiT-1 do not exhibit readily detectable presteady-state relaxations superimposed on the oocyte capacitive charging transient (Fig 2B). Efforts to resolve relaxations have involved subtraction of the step response in control superfusate from the response in the presence of saturating P_i (Ravera, Virkki et al. 2007). Unlike NaPi-IIa/b, charge balance for the subtracted data was not found. This may reflect technical limitations in charge detection, or indicate the presence of another voltage-gated conductance that is sensitive to P_i. The lack of a specific inhibitor and the small magnitude of the associated charge movement have so far precluded more detailed analysis. It is also possible that PiT-1 transduces membrane potential in a different manner from NaPi-IIa/b, or that the charge movements are so fast that they cannot be resolved by the TEVC method. One possibility is that the voltage dependence arises from the translocation of the fully loaded carrier (net charge +1) in a mechanism similar to that proposed for neutral amino acid transporters of the SLC6 family (B^0AT1/SLC6A19) (O'Mara, Oakley et al. 2006). The lack of evidence for

presteady-state relaxations in the presence or absence of Na^+ would further support this possibility.

IV STRUCTURE-FUNCTION RELATIONSHIPS

A. SLC34

1. *Molecular features*

SLC34 proteins belong to a unique class of membrane proteins and appear to share no homology with the other main cation-driven transporter families, even at the bacterial level. They are assumed to be functional monomers based on a study using the rat NaPi-IIa isoform (Kohler, Forster et al. 2000), but there is also evidence they may oligomerise as dimers or possibly tetramers in the membrane (Forster, Hernando et al. 2006; Gisler, Kittanakom et al. 2008; Haito-Sugino, Ito et al. 2012). The primary sequences of the mammalian isoforms vary from 599 amino acids (NaPi-IIc) to approximately 640 amino acids (NaPi-IIa and NaPi-IIb), with differences mainly in the intracellular C-and N-terminal regions and the signature large extracellular linker region (Fig 5A). This linker contains 2 N-glycosylation sites and a disulfide bridge that links the two "halves" of the protein. Cleavage of the disulfide bond of expressed NaPi-IIa leads to loss of function (Lambert, Traebert et al. 2000), but co-expression of the split protein (each containing one of the essential cysteines) results in functional re-assembly (Kohl, Wagner et al. 1998; Ehnes, Forster et al. 2002). The proposed topology of the eukaryotic isoforms comprises 12 α-helices (designated as transmembrane domains (TMDs)) (Fig 5A). This model combines predictions from biochemical and biophysical studies including epitope labeling (Lambert, Traebert et al. 1999), cysteine scanning mutagenesis (see section IV.A.2) and *in vitro* glycosylation assays (Radanovic, Gisler et al. 2006). The C-terminal region is important for targeting, hormonal regulation and protein-protein interactions. For example, the TRL motif in the C-terminal plays a role as a PDZ

binding motif (Hernando, Karim-Jimenez et al. 2001; Karim-Jimenez, Hernando et al. 2001), and a KR motif located in an intracellular linker region (Fig 5A) is critical for parathyroid hormone (PTH) sensitivity (Karim-Jimenez, Hernando et al. 2000).

A salient feature of all SLC34 proteins is the inverted repeat architecture (Fig 5A), which is conserved among SLC34 isoforms and homologs in all phyla (Werner&Kinne 2001). Similar motifs are also found in the 3-D structures of cotransporters with known architecture. Their existence can be interpreted as the structural basis for the alternating access model of carrier-mediated transport. bSuch repeats are considered to arise from gene duplication (Screpanti&Hunte 2007; Abramson&Wright 2009; Boudker&Verdon 2010; Forrest, Kramer et al. 2011).

Fig 5 near here

2. Cysteine mutagenesis

The substituted cysteine accessibility method (SCAM) (Karlin&Akabas 1998) has been extensively applied to the NaPi-IIa isoform to elucidate its structure-function relationships (Lambert, Forster et al. 1999; Lambert, Forster et al. 2001; Kohler, Forster et al. 2002; Ehnes, Forster et al. 2004; Ehnes, Forster et al. 2004; Virkki, Forster et al. 2005). Cys are substituted at selected sites in the protein. If these can be specifically labeled with bulky methanethiosulfonate (MTS) reagents, and a change in transport activity occurs, then this is an indication of the functional importance of that site. By using MTS reagents with a known membrane permeability, sidedness of accessibility to the Cys can be determined. The validity of SCAM rests on the assumption that native Cys are inaccessible, or if labeled, do not alter function (Karlin&Akabas 1998). Complete removal of all 12 native Cys in NaPi-IIa was not possible because of (i) the need to preserve one essential disulfide bridge, and (ii) a progressive decrease in functional activity. Nevertheless, 8 native Cys were successfully removed and the behavior of one novel substituted Cys mutant was recapitulated (Kohler,

Forster et al. 2003), thereby validating using the WT backbone for SCAM. Moreover, using the cut-open oocyte voltage-clamp technique, MTS reagents were applied at the cytosolic interface and no change in WT activity was observed (unpublished experiment, K. Köhler, I. Gautschi, University of Lausanne). This confirmed that native Cys accessible only from the cytosol were also not functionally important. It is assumed that these findings hold for all other isoforms investigated.

So far, SCAM has been applied at sites within 2 predicted external linkers, one TMD and in the re-entrant repeat regions (Fig 5A). Mutants were exposed to membrane permeable and impermeable MTS reagents and the transport properties assayed before and after exposure. By determining the rate of Cys-modification, topological features were confirmed and identified, for example, an α-helical component of the 2nd reentrant segment (TMD9-10, Fig 5B) (Lambert, Forster et al. 2001). In addition, functional changes - either caused by the Cys-mutagenesis itself, or after MTS modification were also observed- thereby giving further insight into functional roles played by different parts of the protein. For example, a Ser-Cys substitution at site 460 (at the top of TMD9, Fig 5A) is well tolerated, although thiol modification results in complete suppression of the cotransport. Nevertheless, the leak mode still operates, and moreover, P_i interacts with the protein (Lambert, Forster et al. 1999). The same loss of cotransport behavior seen after thiol modification of the equivalent mutation in the electroneutral NaPi-IIc (Ser-437) (Ghezzi, Murer et al. 2009), and NaPi-IIb (Ser-448) (Virkki, Murer et al. 2006) confirms the critical importance of this conserved site in all SLC34 members. In another study, reciprocal changes in the voltage dependence of I_{P_i} were found by Cys-mutagenesis and subsequent thiol modification in the linker regions between TMD1 &2 and TMD11 &12 (Ehnes, Forster et al. 2004; Ehnes, Forster et al. 2004). This behavior suggested that specific residues in these linkers may provide flexibility to the protein as it undergoes voltage dependent conformational changes during the transport cycle.

Furthermore, the role of the predicted reentrant segments as codeterminants of the leak and cotransport modes was elucidated by investigating mutants with Cys engineered in the respective repeat regions (Kohler, Forster et al. 2002). This study was recently extended using voltage-clamp fluorometry (Section IV.A.3) and Cys cross-linking assays (Ghezzi, Meinild et al. 2011) to establish that the inverted repeat segments very likely associate physically and can move relative to one another depending on substrate availability.

3. *Voltage-clamp fluorometry*

In contrast to presteady-state assays that report global rearrangements of charges within the protein, voltage-clamp fluorometry (VCF) allows investigation of local conformational changes by labeling engineered cysteines with thiol-reactive fluorophores. Labelled oocytes are voltage clamped and time-resolved fluorescence measurements can be made simultaneously (Fig 6A,B). Changes in the emitted fluorescence intensity (ΔF), induced by substrate and steps in membrane potential, arise from changes in the microenvironment of the fluorophore and therefore report local conformational changes at or near the labeled site (Cha, Zerangue et al. 1998). The temporal resolution is limited only by the speed of charging the oocyte membrane. Substrate (Na^+, Li^+ and P_i) interactions have been explored using VCF applied to the S448C mutant in flounder NaPi-IIb (equivalent to S460C in NaPi-IIa, Fig 5A) to establish that 2 Na^+ ions, (but only one Li^+ ion) interact with the protein before P_i binding and that in the presence of Na^+, P_i interaction induces a conformational change (Virkki, Murer et al. 2006). In this study, a direct correlation between the time course of presteady-state current and ΔF was found for voltage steps to potentials above -40 mV (Fig 6B). This suggested that the charge movement and ΔF report the same physical process in that voltage range.

The power of the VCF technique was further demonstrated by attempting to “map” conformational changes in different regions of the protein. Four sites in the flounder NaPi-IIb

isoform were identified that were labeled with the fluorophore *without* affecting the cotransport function (Virkki, Murer et al. 2006). These constructs permitted the characterization of substrate and voltage-dependent conformational changes associated with specific partial reactions in the complete cotransport cycle. ΔF was measured in: (i) the absence of external Na (restricting the possible states to $0 \leftrightarrow 1$, Fig 4A); (ii) 100 mM Na^+ (restricting the possible states to $0 \leftrightarrow 3$, Fig 4A) and (iii) 100 mM Na^++1 mM P_i (including all states in the cycle, Fig 4A). The complementary ΔF obtained (Fig 6C) suggested that, in response to the same membrane potential change, parts of the protein may experience complementary rearrangements relative to the aqueous medium (Fig 6C). Like the presteady-state charge movments, changes in ΔF showed saturation at potential extremes and the ΔF-V data were fit with a Boltzmann function as for presteady-state charge analysis. The mutants yielded different ΔF -V relationships that depended on the substrate present and, based on the Boltzmann fit parameters, suggested that unique conformational changes occur when either one or two Na^+ ions are bound or when P_i was bound together with Na^+. Moreover, the dependence of ΔF on $[P_i]$ at hyperpolarizing potentials was Michaelian and the $K_{0.5}^{P_i}$ values comparable to those found by electrophysiology.

Fig 6 near here

Recently, the fluorescence technique has been applied to the electroneutral NaPi-IIc by engineering a Cys at the equivalent site (Ser-437) to Ser-460 in NaPi-IIa (Fig 5A) (Ghezzi, Murer et al. 2009). As expected, no voltage-dependent ΔF was detected. However, the emitted fluorescence intensity when the mutant was expressed was found to depend on the composition of the external solution, unlike the background fluorescence. With P_i as the variable substrate, the estimates of $K_{0.5}^{P_i}$ obtained from ^{32}P uptake and ΔF were in excellent agreement. This finding provided strong evidence that despite the lack of cotransport activity after labeling, P_i interactions were still intact and the partial reactions that determine the

apparent affinity for P_i are independent of the substrate translocation. Importantly, this study also revealed that in the absence of P_i, most likely 2 Na^+ ions interact with NaPi-IIc as with the electrogenic isoforms (Eskandari 2009; Ghezzi, Murer et al. 2009). In all these studies, a finding that no ΔF was detected when P_i was applied in the absence of external Na^+, confirms the strict dependence of P_i binding on the presence of Na^+.

4. ***Electrogenicity***

The electroneutral NaPi-IIc (Segawa, Kaneko et al. 2002) provided an important protein tool to identify the molecular determinants of electrogenicity. A sequence comparison identified a conserved trio of amino acids (one of which is an aspartic acid) common to all electrogenic isoforms, located at the bottom of the 4th TMD (Fig 5A). Substitution of these amino acids in the NaPi-IIc re-established electrogenicity, as evidenced by robust P_i-induced steady-state currents, presteady-state relaxations and the predicted 3:1 stoichiometry (Bacconi, Virkki et al. 2005). However, despite the fact that electrogenic and electroneutral isoforms have similar substrate apparent affinities (Table 1), the molecular engineering of NaPi-IIc caused a significantly reduced apparent affinity for both Na^+ and P_i. This suggested that other differences in the amino acid sequences are also important for the kinetic profile. For the complementary experiment, in which the Asp was replaced with a Gly in the NaPi-IIa backbone, electroneutral cotransport was documented, thereby confirming the functional importance of the charged Asp in conferring electrogenicity (Virkki, Forster et al. 2005).

Further insight into the determinants of electrogenicity has come from Cys scanning. Cys-replacement at certain sites throughout the protein resulted in functional mutants that displayed either a hyperpolarizing or depolarizing shift in the voltage dependence relative to the WT (Fig 5A). This was also seen as a concomitant shift in $V_{0.5}$ of the presteady-state *Q-V*. The mutagenesis did not significantly alter their other kinetic parameters (Lambert, Forster et al. 2001; Ghezzi, Meinild et al. 2011). The similarity of their kinetic phenotypes may indicate

that the respective sites are coordinated structurally. It is interesting that only one of these sites contains a charged residue (Fig 5A). In one case (A175C in TMD4, Fig 5A) the hyperpolarizing shift could be simulated using the 10-state model (Fig 4A) by setting a slower forward rate constant for the first Na^+ ion interaction (Ghezzi, Meinild et al. 2011). Given its proximity to the critical Asp (Fig 5A), this finding strongly supports the involvement of this part of the protein in voltage-dependent conformational changes associated with cation binding,

5. Proton interactions

Several structure-function studies have focused on the intrinsic pH dependence of SLC34 proteins- first analyzed in detail for WT NaPi-IIa/b (Forster, Biber et al. 2000). A chimera approach was used to identify the region(s) responsible for conferring pH dependency to NaPi-IIa. This approach was based on the rationale that mouse NaPi-IIb displays a significantly reduced pH dependence compared to mouse NaPi-IIa (de la Horra, Hernando et al. 2000), and led to the identification of a critical region between TMD9 & 10 (Fig 5A). This region contained a triad of neighboring, charged amino acids in NaPi-IIa (REK) that were substituted by an uncharged triad (GNT/A) in mammalian NaPi-IIb. Subsequent mutagenesis involved substitution of the REK triad into NaPi-IIb that restored the NaPi-IIa pH phenotype. Moreover, the pH dependence was abolished when the GNT triad was substituted in NaPi-IIa. These findings were also supported by the behavior of Cys-substituted NaPi-IIa mutants that displayed decreased pH sensitivity when any of the three residues was replaced by a Cys (Lambert, Forster et al. 2001). However, based on more recent studies and subsequent cloning of other SLC34 isoforms, it is unlikely that this motif represents the only proton interacting site in NaPi-IIa for several reasons. First, although the REK motif is conserved among all NaPi-IIa that display a strong pH dependence (Busch, Waldegger et al. 1994; Busch, Wagner et al. 1995; Hartmann, Wagner et al. 1995; Forster,

Hernando et al. 1998; Forster, Biber et al. 2000), it is present neither in the Zebra fish NaPi-IIb1 (Nalbant, Boehmer et al. 1999), nor NaPi-IIc, both of which show the phenotypically strong NaPi-IIa pH dependency (Segawa, Kaneko et al. 2002). Second, in the flounder NaPi-IIb that shows strong pH dependence (Forster, Biber et al. 2000) and the zebra fish NaPi-IIb2, that shows weaker pH dependence (Graham, Nalbant et al. 2003), the arginine is replaced by a neutral alanine. Third, an electrophysiological study on mouse NaPi-IIb (Forster, Virkki et al. 2006) reported that $K_{0.5}^{P_i}$ was ~5-fold smaller than for NaPi-IIa isoforms (see Table). Therefore, for pH < 7, although the availability of divalent P_i is decreased, the low $K_{0.5}^{P_i}$ can explain the apparent insensitivity of the mouse NaPi-IIb isoform to acid pH. Given the variability of residues at the equivalent sites among the different isoforms, it is therefore likely that other residues also play a role in determining both pH sensitivity and apparent P_i affinity.

B. SLC20

1. ***Molecular features***

A 10 TMD topology was proposed for the human receptor of the gibbon ape virus (SLC20A1/PiT-1) based on hydrophobicity predictions (O'Hara, Johann et al. 1990). With subsequent sequencing of homologous receptors in other species, and the recognition that these proteins serve the dual function of viral receptor and P_i transporter, more detailed topological analyses led to the current secondary topology model of PiT-2 (SLC20A2) (Fig 7). These studies used a combination of *in vitro* glycosylation assays, epitope tagging, cysteine scanning and sequence comparisons of all related family members (Salaun, Rodrigues et al. 2001; Farrell, Tusnady et al. 2009; Bottger&Pedersen 2011). The current model predicts a 12 TMD structure, but in contrast to SLC34 family proteins, the N- and C-termini are both extracellular. The topology is characterized by the large intracellular linker region between predicted TMD7 &8. An “inverted topology” containing amino acid blocks

that are also conserved among all family members has been identified, which are referred to as PD1131 homology domains (Salaun, Rodrigues et al. 2001) and comprise stretches of identical residues designated as PiT signature sequences (Bottger&Pedersen 2005). Previously, much of the structure-function interest in these proteins has focused on identifying those parts responsible for viral receptor function (Pedersen, Johann et al. 1995; Pedersen, van Zeijl et al. 1997; Farrell, Russ et al. 2002; Feldman, Farrell et al. 2004; Bottger&Pedersen 2005; Farrell, Tusnady et al. 2009; Bottger&Pedersen 2011). For example, a PiT-2 mutant that lacked the large intracellular loop together with the preceding TMD6 &7 still supported viral entry (Bottger&Pedersen 2004). A recent study reported functional P_i transport when most of the intracellular loop was deleted (Bottger&Pedersen 2011) (Fig 7). PiT-1 and PiT-2 differ in the location of their putative virus binding sites (e.g. the 1st extracellular loop for PiT-2 (Feldman, Farrell et al. 2004), and the 4th extracellular loop for PiT-1 (Johann, van Zeijl et al. 1993)).

Several residues critical for transport function have been identified in the PiT-2 sequence by mutagenesis (Bottger&Pedersen 2002; Bottger&Pedersen 2005; Bottger, Hede et al. 2006). Two glutamate residues (E55, E575 in human PiT-2, Fig. 7) that are conserved in PiT-1 and PiT-2, as well as many related phosphate permeases from bacteria and fungi, were replaced with glutamines. Transport function was reduced significantly, while the viral receptor function remained unaffected (Bottger&Pedersen 2002). In another study, two conserved aspartic acids in the PiT family signature sequences (D28 and D506, Fig 7), were mutated to asparagines and transport function was again suppressed (Bottger&Pedersen 2005), whereas mutations at E68 and D76 within the predicted first extracellular loop (Fig 7) only partially affected function. Functional assays in these studies were by uptake and although membrane expression levels were confirmed by biotinylation assays, no detailed information on the effects of the mutations on transport kinetics was reported.

Fig 7 near here

2. *Cysteine mutagenesis*

An extensive Cys scanning of PiT-1 has been undertaken in the context of determining its secondary topology features and virus binding interaction (Farrell, Tusnady et al. 2009). The predicted topology from this study is very similar to the 12 TMD model for PiT-2 (Fig 7). We have recently performed a Cys-scanning study on the first predicted extracellular loop of the *Xenopus* isoform of PiT-1 that contains a glutamine and aspartic acid previously identified to be critical for cotransport function (Bottger&Pedersen 2005). Exposure of the WT PiT-1 to MTS reagents showed no change in electrogenic activity- a finding that confirms that none of the 5 native Cys was in a functionally sensitive position or readily accessible. Twelve sites were replaced individually with a Cys, and the mutants were expressed in oocytes as described above for SLC34. Whereas Cys-substitution was well tolerated at all sites, ^{32}P uptake was significantly suppressed for 6 mutants after MTS exposure. Thus this linker region is possibly near the substrate binding sites or associated with the transport pathway itself (manuscript in preparation, S. Ravera, I C. Forster).

V. FUTURE PERSPECTIVES

The characterization of the transport kinetics of WT SLC20 and SLC34 isoforms expressed in *Xenopus* oocytes has revealed fundamental differences in their transport kinetics. These differences are highlighted by the lack of detectable presteady-state charge movement for SLC20 proteins. For the electrogenic SLC34 isoforms (NaPi-IIa and NaPi-IIb), these relaxations display many of the characteristics found for electrogenic cotransporters from other SLC families (e.g. SGLT, NIS (SLC5) (e.g. (Loo, Hazama et al. 1993; Eskandari, Loo et al. 1997; Loo, Eskandari et al. 2002)) and GAT (SLC6) (e.g. (Mager, Naeve et al. 1993; Sacher, Nelson et al. 2002; Meinild&Forster 2012)).The similarities suggest that a common

mechanism, which underlies the manner whereby the free energy of the membrane potential is transduced to drive cotransport, is shared among these families. For SLC20 proteins, the absence of detectable presteady-state charge movements suggests that the final translocation of the fully loaded protein is electrogenic. However, this notion requires further investigation. Moreover, further investigation of the SLC20 family kinetics would benefit from having a specific inhibitor.

At present, the kinetic model developed for electrogenic SLC34 proteins can successfully account for the forward mode of cotransport. However, the intact whole oocyte preparation severely limits the experimental manipulations necessary to characterise fully the reverse cycle and investigate substrate interactions at the cytosolic interface. Future work should therefore aim at characterizing the internal partial reactions using for example, excised giant membrane patches or the cut-open oocyte technique, as has been applied to SGLT1(Eskandari, Wright et al. 2005) and GAT1 (Hilgemann&Lu 1998).

The structure-function studies carried out to date exemplify what can be achieved in the absence of 3-D structural information. The combination of a variety of approaches including bioinformatics, SCAM and VCF has provided important insights into the structure-function relationships of SLC34 proteins and should be extended to the SLC20 family. Structural predictions made by Cys-scanning , taken together with TMD cross-linking assays, can identify features similar to those revealed in the 3-D structures, as exemplified by studies on lactose permease (LacY) (Kaback, Sahin-Toth et al. 2001; Abramson, Smirnova et al. 2003) and the GAT1 bacterial homolog $LeuT_{Aa}$ (Yamashita, Singh et al. 2005; Kanner 2006). This provides validation for the further use of these strategies for proteins with as yet unresolved structures. At the same time, the kinetic analysis of engineered Cys-mutants has led to the identification of functionally important sites, underscoring the continued relevance of functional studies. In this context, the application of the fluorometric assays has already

shown its potential as tool to study the dynamics of transporters in their native environment and complement conventional assays.

Acknowledgements

Work from our own laboratories was supported in part by funding from the Swiss National Science Foundation. The authors thank the following past and present members for their invaluable contributions to many of the reported studies: Olga Andrini, Andrea Bacconi, Carmen de la Horra, Colin Ehnes, Chiara Ghezzi, Katja Köhler, Georg Lambert, Anne-Kristine Meinild, Monica Patti, Silvia Ravera and Leila Virkki.

Table

Kinetic properties of SLC34 and SCL20 proteins expressed in *Xenopus* oocytes

Family	SLC34			SLC20
Isoform	NaPi-IIa (SLC34A1)	NaPi-IIb (SLC34A2)	NaPi-IIc (SLC34A3)	PiT-1 (PiT-2) (SLC20A1/A2)
P_i species preferred	HPO_4^{2-} [a]	HPO_4^{2-} [a]	HPO_4^{2-} [b]	$H_2PO_4^{-}$ [c]
Driving cations	Na^+ (Li^+[d])	Na^+(Li^+[d])	Na^+[e]	Na^+, Li^+ [c]
Electrogenicity (charge/cycle)	1[a]	1[a]	0[e]	1[c]
Stoichiometry (Na:P_i)	3:1 [a,f]	3:1[a]	2:1[b]	2:1[c]
Presteady-state currents	Yes [g,f]	Yes [h,d,j]	No [b]	n.d
$K_{0.5}^{Pi}$ (μM)	50[f] ,54[g]	250[k] ,7[h], 29[i],31[j]	70[e], 80[l]	120[c], 24[m], 25[m]
$K_{0.5}^{Na}$ (mM)	40[f], 50[g]	25[h], 42[i], 46[j], 67[k]	48[e], 43[l]	50[c]
pH dependence (pH↓)	strong[g,f,n]	strong[h,j,k], weak[i]	strong[e]	weak[c]
Turnover (s^{-1}) (-60 mV)	4[g]	9[o], 13[j]	n.d	n.d
Concentrating capacity (10:1 Na gradient, -60 mV)	10000:1	10000:1	100:1	1000:1
Arsenate (K_i^{As}) (mM)	1.08[p]	0.05[p]	1.01[p]	3.61[q] (3.95[q])
PFA (K_i^{PFA}) (mM)	1.05[p]	0.16[p]	0.9[p]	2.71[q] (4.63[q])
Leak (% of I_{P_i},1 mM P_i) (-100mV)	~10[g,r]	~5[r]	n.d	n.d

n.d.: not determined; PFA: phosphonoformic acid

[a]rat NaPi-IIa, flounder NaPi-IIb (Forster, Loo et al. 1999),

[b]mouse NaPi-IIc (Bacconi, Virkki et al. 2005)

[c]*Xenopus* PiT-1(Ravera, Virkki et al. 2007)

[d]flounder NaPi-IIb (Andrini, Meinild et al. 2012)

[e]human NaPi-IIc (Segawa, Kaneko et al. 2002)

[f]human NaPi-IIa (Virkki, Forster et al. 2005)

[g]rat NaPi-IIa (Forster, Hernando et al. 1998)

[h] mouse NaPi-IIb (Forster, Virkki et al. 2006)

[i]zebra fish NaPi-IIb2 (Graham, Nalbant et al. 2003)

[j]flounder NaPi-IIb (Forster, Wagner et al. 1997)

[k]zebra fish NaPi-IIb1 (Nalbant, Boehmer et al. 1999)

[l]mouse NaPi-IIc (Ghezzi, Murer et al. 2009)

[m]human PiT-1, rat PiT-2 (Kavanaugh, Miller et al. 1994)

[n]rat NaPi-IIa (Busch, Waldegger et al. 1994)

[o]L.V. Virkki, unpublished

[p]rat NaPi-IIa/b/c (Villa-Bellosta&Sorribas 2008)

[q]rat PiT-1,-2 (Villa-Bellosta, Bogaert et al. 2007)

[r]rat NaPi-IIa, flounder NaPi-IIb (Andrini, Ghezzi et al. 2008)

Figure Legends

FIGURE 1. Phylogenetic trees of SLC34 and SLC20 families showing selected members

(A) SLC34 (type II Na^+/P_i transporters). The following sequences were used: mouse NaPi-IIb (AAC80007), rat NaPi-IIb (NP_445832), human NaPi-IIb (AAF31328), *X. laevis* NaPi-IIb (AAF21135), flounder NaPi-IIb (AAB16821), zebra fish NaPi-IIb (AF121796), mouse NaPi-IIa (AAC52361), rat NaPi-IIa (NP_037162), human NaPi-IIa (AAA36354), mouse NaPi-IIc (NP_543130), rat NaPi-IIc (NP_647554), human NaPi-IIc (NP_543153) , *Vibrio cholerae* NaPi-II_(230325). Boxed members are electrogenic.

(B) SLC20 (type III Na^+/P_i transporters). The following sequences were used: human PiT-1 (NM_005415), mouse PiT-1 (AAB31458), rat PiT-1 (NM_031148), *X. laevis* PiT-1 (AAH59957), zebra fish PiT-1 (NM_213179), mouse PiT-2 (NM_011394), rat PiT-2 (NM_017223), human PiT-2 (NM_006749), *X. laevis* PiT-2 (BC084098), *Arabidopsis thaliana* Pht2;1 (NM_113565), *Medicago truncatula* Pht2;1 (AAN46087), *Plasmodium falciparum* PfPiT (AJ580003), *Neurospora crassa* Pho-4 (XM_954396), *Escherichia coli* PitA (NC_002655), *E.coli* PitB (NC_000913). Arrows indicate members with confirmed electrogenic behavior.

Amino acid sequences were aligned using ClustalW. Genbank accession numbers are listed in parentheses. Insets in each panel depict consensus secondary topology of mammalian proteins. Inverted repeat regions indicated by dark shading. Data redrawn and modified from (Virkki, Biber et al. 2007), with permission.

FIGURE 2. Overview of transport mechanisms of SLC34 and SLC20 proteins

(A) SLC34. *Left panel*: Cartoon of substrate interactions with electrogenic (NaPi-IIa/b) (*upper*) and electroneutral (NaPi-IIc) (*lower*) isoforms. Driving forces are indicated for the normal transport cycle. Substrates interact in an ordered sequence (indicated by numbers on

cartoon) in which 2 Na^+ ions bind sequentially, followed by divalent P_i and a 3rd Na^+ ion. For electrogenic NaPi-IIa/b, an effective negative charge, intrinsic to the protein confers voltage dependence to the transport cycle (Section V.A.4). Movement of this charge leads to binding of the 1st Na^+ ion and subsequent translocation together with the other substrates, giving a 3:1 Na^+:P_i stoichiometry. After substrate release to the cytosol, the intrinsic charge again senses the transmembrane field, leading to a voltage-dependent reorientation of the empty carrier. For the electroneutral NaPi-IIc, a Na^+ ion first binds like NaPi-IIa/b, but is not translocated (Ghezzi, Murer et al. 2009), giving a 2:1 Na^+:P_i stoichiometry.

Center panel: Original current recordings from a voltage clamped oocyte expressing flounder NaPi-IIb in solution containing 100 mM Na^+ (*left*) and 100 mM Na^+ +1 mM P_i (*right*). The voltage was stepped from -160 to +80 mV in 40 mV increments. Arrows indicate presteady-state relaxations that are suppressed in the presence of P_i (see Section III.B.2). Dashed line indicates zero current level. Bars indicate steady-state (open) and presteady-state (filled) regions of the records.

Right panel: Steady-state P_i-dependent current (I_{P_i}) as a function of voltage for different external cations (at 100 mM) for an oocyte expressing flounder NaPi-IIb. Each data point is the difference between the oocyte holding current at the indicated membrane potential with and without 1 mM P_i (pH 7.4). No significant inward current is recorded when Na^+ is replaced with choline or Li^+. The dashed line indicates the deviation from linearity at extreme membrane potentials.

(B) SLC20. *Left panel*: Cartoon of substrate interactions with PiT-1/2. Driving forces are indicated for the normal transport cycle. Substrate interactions comprise an initial binding of one Na^+ ion, followed by a random interaction of monovalent P_i and a 2nd Na^+ ion (Ravera, Virkki et al. 2007). Reorientation of the loaded carrier leads to substrate release in the cytosol. Neither intrinsic charge movements nor voltage-dependent Na^+ ion interactions have been

detected experimentally; therefore, the translocation step itself is hypothesized to confer voltage dependence.

Center panel: Original current recordings from an oocyte expressing *Xenopus* PiT-1 superfused with 100 mM Na^+ (left) and 100 mM Na^+ +1 mM P_i (right). The voltage was stepped from -160 to +40 mV in 20 mV increments. Note that no presteady-state relaxations are visible. Dashed line indicates zero current level. Bars indicate steady-state (open) and presteady-state (filled) regions of current records.

Right panel: Steady-state P_i-dependent current (I_{P_i}) plotted as a function of voltage for different driving cations (at 100 mM) for an oocyte expressing *Xenopus* PiT-1. No significant inward current is recorded when Na^+ is replaced with choline, whereas currents are reduced by ~85% for V<0 mV when Na^+ is replaced by Li^+.

Data redrawn and modified from (Virkki, Biber et al. 2007), with permission.

FIGURE 3. Presteady-state kinetics of electrogenic SLC34 proteins

(A) Current recordings from a representative voltage- clamped oocyte expressing flounder NaPi-IIb in response to voltage steps from -60 mV to potentials in the range -180 mV to +80 mV in 20 mV increments for superfusion conditions indicated. Endogenous steady-state currents and capacitive transients were eliminated by baseline subtraction and curve fitting.

(B) Relaxation time constant (τ) (*left*) and normalised charge (Q_{norm}) (*right*) plotted as a function of membrane potential (V) for a representative voltage-clamped oocyte expressing flounder NaPi-IIb with superfusion conditions indicated. Arrows on Q_{norm}-V data indicate the state occupancy at the voltage limits according to the scheme in (C). Continuous traces are fits using Eqn 3.

(C) Cartoon depicting a 4 state model that can account for the data in (B). Charge movements in response to a step change in membrane voltage arise from the movement of a lumped

negative charge intrinsic to the protein and 2 Na^+ ions moving to their binding sites within the transmembrane electric field. At very positive potentials, all proteins occupy state 0, and at very negative potentials state 3 is occupied. Fitting the Q_{norm}-V data with a single Boltzmann function assumes a two-state model. At intermediate potentials, the proteins would be distributed among the 4 states according to the rate constants for the 3 partial reactions. Effective valence of each partial reaction is indicated, based on data analysis and simulations (Andrini, Meinild et al. 2012).

FIGURE 4. A 10-state model for simulating steady-state and presteady-state kinetics of electrogenic SLC34 proteins

(A) Scheme of 10-state model. The numbered "states" represent unique conformations of the protein that either favor substrate interactions from the external membrane face (1↔5) or on the inside (0↔6), consistent with an alternating access mechanism. The leak pathway is hypothesized to be 2↔9. Each transition is assumed to obey pseudo 1st order kinetics, and for generality, non-rapid equilibrium conditions were assumed (see (Parent, Supplisson et al. 1992; Loo, Eskandari et al. 2002)). The scheme is symmetric, whereby substrate interactions from the external and internal membrane surfaces follow the same order, although this has not yet been established experimentally. To simplify the modelling, the transitions between state 6 and 0 are lumped into a single partial reaction (Andrini, Meinild et al. 2012). All voltage dependencies for the cotransport cycle can be accounted for by partial reactions that precede P_i binding (Fig 3C). For the simulations, the 2nd Na^+ interaction (2↔3) was assumed to be electroneutral. This is consistent with a proposed model for NaPi-IIc in which the first Na^+ ion is not translocated and the lack of experimental evidence for voltage-dependent transitions (Ghezzi, Murer et al. 2009). More recent studies suggest that for the electrogenic NaPi-IIb, this partial reaction also involves charge movement (Andrini, Meinild et al. 2012). Li^+ ions

compete for occupancy of the 1st Na^+ binding site, and in doing so, can replace one of the 3 Na^+ ions that participate in cotransport (Andrini, Meinild et al. 2012). Numerical simulations using this model were performed by solving the set of differential equations that describe the transitions between states. Rate constants for transitions involving charge movement were defined according to simple symmetrical barrier models based on Eyring transition state theory (see (Ghezzi, Meinild et al. 2011; Andrini, Meinild et al. 2012) for more details).
(B) Normalized steady-state I_{P_i} plotted as a function of membrane potential comparing representative data from an oocyte expressing flounder NaPi-IIb (filled squares) and simulated data (open squares). Data are normalized to I_{P_i} at -100 mV.

(C) Comparison of Boltzmann fit parameters derived from simulations (open squares) of *Q-V* (in absence of P_i) with representative data obtained from oocytes expressing flounder NaPi-IIb (filled squares). The normalised Q_{max} is reasonably independent of $[Na^+]$ except for low $[Na^+]$ where the single Boltzmann assumption breaks down. The magnitude and variation of the apparent valence (slope factor of Boltzmann function (Eqn 3)) with $[Na^+]$ similarly reflects the fact that charge movement arises from 3 partial reactions. The limiting slope of the logarithmic plot of $V_{0.5}$ vs $[Na^+]$ is ≈120 mV/decade, which is consistent with 2 Na^+ ions binding to the protein.

FIGURE 5. Topology and structure-function features of SLC34 proteins

(A) Topology model based on rat NaPi-IIa sequence. Transmembrane domains (1-12) were assigned according to (Radanovic, Gisler et al. 2006). The model was drawn using TOPO2 software (http://www.sacs.ucsf.edu/TOPO/topo.html). Enlarged symbols indicate sites of significant structure-function importance. *Pink*: identical residues in the re-entrant repeats; *green*: sites when mutated to a Cys that are externally accessible; *blue*: sites when mutated to a cysteine that are internally accessible; *purple*: sites externally inaccessible; *red*: sites critical

for electrogenicity; *orange*: sites important for regulation and targeting; *black*: native Cys; *grey*: determinants of pH dependence. An essential disulfide bridge in the large extracellular loop is indicated (*dashed line*). Two N-glycosylation sites have been identified in the linker between TMD5 & 6. Boxed "-" and "+" refer to sites that result in mutant transporters with a hyperpolarizing or depolarizing shift, respectively, in their voltage dependence when a Cys is substituted. Modified and updated from (Virkki, Biber et al. 2007), with permission.

(B) External accessibility determined by cysteine scanning. Summary of regions in the protein explored so far. Ordinate represents the modification rate (on logarithmic scale) of the Cys at the respective site and gives an indirect measure of its accessibility. These data suggest that the top of TMD9 is more accessible than the two outer linker regions (TMD1↔2 and TMD 11↔12), and the linker between TMD1↔2 is more accessible than the linker between TMD11↔12. Empty symbols indicate sites that were accessible, but resulted in unchanged transport behavior. Modified from (Ehnes, Forster et al. 2004), with permission.

Inset: detail of region in TMD9 that shows the periodicity of an α-helix. From (Lambert, Forster et al. 2001) with permission. This region is hypothesized to form part of a re-entrant segment that physically associates with TMD4 (Ghezzi, Meinild et al. 2011).

FIGURE 6. Application of voltage-clamp fluorometry to SLC34 structure-function studies

(A) Schematic of a typical voltage-clamp fluorometry (VCF) setup for *Xenopus* oocytes. The oocyte membrane is voltage clamped using a conventional two-electrode voltage-clamp (TEVC), and placed in a chamber with a transparent bottom to allow fluorophores to be excited and their emission measured. For more technical information see (Cha, Zerangue et al. 1998; Virkki, Murer et al. 2006).

(B) *Upper panel*: Voltage steps evoke presteady-state relaxations (I_{pss}) and changes in emitted fluorescence intensity (ΔF) recorded simultaneously on the same oocyte expressing the flounder NaPi-IIb mutant (S448C) labelled with the fluorophore MTS-TAMRA. *Lower panel*: a parametric plot of I_{pss} against ΔF. The linear relationships found for V>-40 mV indicate that the time course of presteady-state relaxation and change in fluorescence intensity correlate. This suggests that the voltage-dependent charge displacement reported by I_{pss} and changes in the fluorophore micro-environment reported by ΔF reflect the same protein conformational changes in this membrane potential range. Modified and redrawn from (Virkki, Murer et al. 2006).

(C) The voltage-dependent ΔF detected by labeling 2 sites in the N-terminal half of the NaPi-IIb protein (mutant S155C, S226C) are complementary to ΔF recorded from 2 sites in the C-terminal half (Q319C, E451C). This behavior suggests that complementary rearrangements of the protein occur relative to the aqueous medium. (Data adapted and redrawn from (Virkki, Murer et al. 2006)).

FIGURE 7. Topology and structure-function features of SLC20 proteins

This topology model for mammalian SLC20 proteins is based on the human PiT-2 sequence. The 12 predicted TMDs were assigned according to (Salaun, Rodrigues et al. 2001). The model was drawn using TOPO2 software (http://www.sacs.ucsf.edu/TOPO/topo.html). Residues important for SLC20 function that have been identified by mutagenesis (Bottger&Pedersen 2004; Salaun, Marechal et al. 2004; Bottger&Pedersen 2005) are shown enlarged. *Blue*: PD1131 homology domains (Salaun, Rodrigues et al. 2001). Two regions involving the large intracellular loop have been deleted: the ΔL183-V483 deletion causes loss of transport function with partially compromised viral receptor function (*green*) and the ΔR254-V483 leaves transport function intact but compromises viral receptor function

(*orange*) (Bottger&Pedersen 2011). Acidic residues important for transport function (D28, E55, D506, E575) (*red*) and those not critical for transport function (E68, D78, E91) (*pink*) are indicated. The protein is N-glycosylated at Asp-81. A region in the 1st extracellular loop of PiT-1, also conserved in PiT-2 was subjected to SCAM, and sites accessible from the external medium have been identified (Ravera, S and Forster, I.C. manuscript in preparation).

Footnote 1

Unlike ion channels, for which the current through a single channel is typically on the order of pA or more, the inherently slow turnover rate of cotransporters implies that for a single charge translocated at 100 s^{-1}, the current per protein will be ≈0.016 fA.

References

Abramson, J., Smirnova, I., et al. (2003). "The lactose permease of Escherichia coli: overall structure, the sugar-binding site and the alternating access model for transport." *FEBS Letters 555*(1): 96-101.

Abramson, J.&Wright, E. M. (2009). "Structure and function of Na(+)-symporters with inverted repeats." *Current Opinion in Structural Biology 19*(4): 425-32.

Andrini, O., Ghezzi, C., et al. (2008). "The leak mode of type II Na(+)-P(i) cotransporters." *Channels (Austin) 2*(5): 346-57.

Andrini, O., Meinild, A. K., et al. (2012). "Lithium interactions with Na+-coupled inorganic phosphate cotransporters: insights into the mechanism of sequential cation binding." *Am J Physiol Cell Physiol 302*(3): C539-54.

Bacconi, A., Ravera, S., et al. (2007). "Temperature dependence of steady-state and presteady-state kinetics of a type IIb Na+/P i cotransporter." *Journal of Membrane Biology 215*(2-3): 81-92.

Bacconi, A., Virkki, L. V., et al. (2005). "Renouncing electrogenicity is not free of charge: switching on electrogenicity in a Na^+-coupled phosphate cotransporter." *Proceedings of the National Academy of Sciences of the United States of America 102*: 12606-11.

Bai, L., Collins, J. F., et al. (2000). "Cloning and characterization of a type III Na-dependent phosphate cotransporter from mouse intestine." *American Journal of Physiology 279*(4): C1135-43.

Barac-Nieto, M., Alfred, M., et al. (2002). "Basolateral phosphate transport in renal proximal-tubule-like OK cells." *Exp Biol Med (Maywood) 227*(8): 626-31.

Beck, L., Karaplis, A. C., et al. (1998). "Targeted inactivation of Npt2 in mice leads to severe renal phosphate wasting, hypercalciuria, and skeletal abnormalities." *Proceedings of the National Academy of Sciences of the United States of America 95*(9): 5372-7.

Beck, L., Leroy, C., et al. (2010). "The phosphate transporter PiT1 (Slc20a1) revealed as a new essential gene for mouse liver development." *PLoS One 5*(2): e9148.

Beene, L. C., Halluer, J., et al. (2011). "Pentavalent arsenate transport by zebrafish phosphate transporter NaPi-IIb1." *Zebrafish 8*(3): 125-31.

Bellocchio, E. E., Reimer, R. J., et al. (2000). "Uptake of glutamate into synaptic vesicles by an inorganic phosphate transporter." *Science 289*(5481): 957-60.

Bergwitz, C., Roslin, N. M., et al. (2006). "SLC34A3 Mutations in Patients with Hereditary Hypophosphatemic Rickets with Hypercalciuria Predict a Key Role for the Sodium-Phosphate Cotransporter NaPi-IIc in Maintaining Phosphate Homeostasis." *Am J Hum Genet 78*(2): 179-92.

Berndt, T.&Kumar, R. (2007). "Phosphatonins and the regulation of phosphate homeostasis." *Annu Rev Physiol 69*: 341-59.

Berndt, T. J., Knox, F.G. (1992). Renal regulation of phosphate excretion. The Kidney: Physiology and Pathophysiology. D. W. Seldin, Giebisch, G. New York, Raven Press**:** 2511-2526.

Berner, W., Kinne, R., et al. (1976). "Phosphate transport into brush-border membrane vesicles isolated from rat small intestine." *Biochemical Journal 160*(3): 467-74.

Biber, J., Hernando, N., et al. (2009). "Regulation of phosphate transport in proximal tubules." *Pflugers Archiv. European Journal of Physiology 458*(1): 39-52.

Bottger, P., Hede, S. E., et al. (2006). "Characterization of transport mechanisms and determinants critical for Na+-dependent Pi symport of the PiT-family paralogs, human PiT1 and PiT2." *American Journal of Physiology 291*: C1377-C1387.

Bottger, P.&Pedersen, L. (2002). "Two highly conserved glutamate residues critical for type III sodium-dependent phosphate transport revealed by uncoupling transport function from retroviral receptor function." *J Biol Chem 277*(45): 42741-7.

Bottger, P.&Pedersen, L. (2004). "The central half of Pit2 is not required for its function as a retroviral receptor." *J Virol 78*(17): 9564-7.

Bottger, P.&Pedersen, L. (2005). "Evolutionary and experimental analyses of inorganic phosphate transporter PiT family reveals two related signature sequences harboring highly conserved aspartic acids critical for sodium-dependent phosphate transport function of human PiT2." *Febs J 272*(12): 3060-74.

Bottger, P.&Pedersen, L. (2011). "Mapping of the minimal inorganic phosphate transporting unit of human PiT2 suggests a structure universal to PiT-related proteins from all kingdoms of life." *BMC Biochem 12*: 21.

Boudker, O.&Verdon, G. (2010). "Structural perspectives on secondary active transporters." *Trends in Pharmacological Sciences 31*(9): 418-26.

Broer, S., Schuster, A., et al. (1998). "Chloride conductance and Pi transport are separate functions induced by the expression of NaPi-1 in Xenopus oocytes." *Journal of Membrane Biology 164*(1): 71-7.

Busch, A., Waldegger, S., et al. (1994). "Electrophysiological analysis of Na^+/P_i cotransport mediated by a transporter cloned from rat kidney and expressed in Xenopus oocytes." *Proceedings of the National Academy of Sciences of the United States of America 91*(17): 8205-8.

Busch, A. E., Schuster, A., et al. (1996). "Expression of a renal type I sodium/phosphate transporter (NaPi-1) induces a conductance in Xenopus oocytes permeable for organic and inorganic anions." *Proceedings of the National Academy of Sciences of the United States of America 93*(11): 5347-51.

Busch, A. E., Wagner, C. A., et al. (1995). "Properties of electrogenic P_i transport by a human renal brush border Na^+/P_i transporter." *Journal of the American Society of Nephrology 6*(6): 1547-51.

Cecil, D. L., Rose, D. M., et al. (2005). "Role of interleukin-8 in PiT-1 expression and CXCR1-mediated inorganic phosphate uptake in chondrocytes." *Arthritis and Rheumatism 52*(1): 144-54.

Cha, A., Zerangue, N., et al. (1998). "Fluorescence techniques for studying cloned channels and transporters expressed in Xenopus oocytes." *Methods Enzymol 296*: 566-78.

Collins, J. F., Bai, L., et al. (2004). "The SLC20 family of proteins: dual functions as sodium-phosphate cotransporters and viral receptors." *Pflugers Archiv - European Journal of Physiology 447*(5): 647-52.

Corut, A., Senyigit, A., et al. (2006). "Mutations in SLC34A2 cause pulmonary alveolar microlithiasis and are possibly associated with testicular microlithiasis." *Am J Hum Genet 79*(4): 650-6.

Daram, P., Brunner, S., et al. (1999). "Pht2;1 encodes a low-affinity phosphate transporter from Arabidopsis." *Plant Cell 11*(11): 2153-66.

de la Horra, C., Hernando, N., et al. (2000). "Molecular determinants of pH sensitivity of the type IIa Na/P_i cotransporter." *Journal of Biological Chemistry 275*(9): 6284-7.

Ehnes, C., Forster, I. C., et al. (2004). "Structure-function relations of the first and fourth extracellular linkers of the type IIa Na^+/P_i cotransporter: II. Substrate interaction and voltage dependency of two functionally important sites." *Journal of General Physiology 124*: 489-503.

Ehnes, C., Forster, I. C., et al. (2004). "Structure-function relations of the first and fourth predicted extracellular linkers of the type IIa Na^+/Pi cotransporter: I. Cysteine scanning mutagenesis." *Journal of General Physiology 124*(5): 475-88.

Ehnes, C., Forster, I. C., et al. (2002). "Functional studies on a split type II Na/Pi-cotransporter." *Journal of Membrane Biology 188*(3): 227-236.

Eskandari, S. (2009). "Remarkable commonalities of electrogenic and electroneutral Na+-phosphate cotransporters." *J Physiol 587*(Pt 17): 4131-2.

Eskandari, S., Loo, D. D., et al. (1997). "Thyroid Na^+/I^- symporter. Mechanism, stoichiometry, and specificity." *Journal of Biological Chemistry 272*(43): 27230-8.

Eskandari, S., Wright, E. M., et al. (2005). "Kinetics of the reverse mode of the Na+/glucose cotransporter." *J Membr Biol 204*(1): 23-32.

Farrell, K. B., Russ, J. L., et al. (2002). "Reassessing the role of region A in Pit1-mediated viral entry." *Journal of Virology 76*(15): 7683-93.

Farrell, K. B., Tusnady, G. E., et al. (2009). "New structural arrangement of the extracellular regions of the phosphate transporter SLC20A1, the receptor for gibbon ape leukemia virus." *Journal of Biological Chemistry 284*(43): 29979-87.

Feldman, S. A., Farrell, K. B., et al. (2004). "Identification of an extracellular domain within the human PiT2 receptor that is required for amphotropic murine leukemia virus binding." *Journal of Virology 78*(2): 595-602.

Forrest, L. R., Kramer, R., et al. (2011). "The structural basis of secondary active transport mechanisms." *Biochimica et Biophysica Acta 1807*(2): 167-88.

Forster, I. (2007). Electrogenic phosphate transport across renal epithelia: mechanistic insights from experiments and simulations. Workshop 5: the kidney: cellular, tubular and vascular physiology. Mathematical Biosciences Institute, OSU.

Forster, I., Hernando, N., et al. (1998). "The voltage dependence of a cloned mammalian renal type II Na^+/P_i cotransporter (NaPi-2)." *Journal of General Physiology 112*(1): 1-18.

Forster, I., Hernando, N., et al. (2011). "Phosphate transporters in renal, gastrointestinal, and other tissues." *Adv Chronic Kidney Dis 18*(2): 63-76.

Forster, I. C., Biber, J., et al. (2000). "Proton-sensitive transitions of renal type II Na^+-coupled phosphate cotransporter kinetics." *Biophysical Journal 79*(1): 215-30.

Forster, I. C., Hernando, N., et al. (2006). "Proximal tubular handling of phosphate: A molecular perspective." *Kidney Int 70*(9): 1548-59.

Forster, I. C., Loo, D. D., et al. (1999). "Stoichiometry and Na^+ binding cooperativity of rat and flounder renal type II Na^+-P_i cotransporters." *American Journal of Physiology 276*(4 Pt 2): F644-9.

Forster, I. C., Virkki, L. V., et al. (2006). "Electrogenic kinetics of a mammalian intestinal Na^+/P_i-cotransporter." *Journal of Membrane Biology 212*: 177-190.

Forster, I. C., Wagner, C. A., et al. (1997). "Electrophysiological characterization of the flounder type II Na^+/P_i cotransporter (NaPi-5) expressed in Xenopus laevis oocytes." *Journal of Membrane Biology 160*(1): 9-25.

Frei, P., Gao, B., et al. (2005). "Identification and localization of sodium-phosphate cotransporters in hepatocytes and cholangiocytes of rat liver." *American Journal of Physiology 288*(4): G771-8.

Ghezzi, C., Meinild, A. K., et al. (2011). "Voltage- and substrate-dependent interactions between sites in putative re-entrant domains of a Na(+)-coupled phosphate cotransporter." *Pflugers Archiv. European Journal of Physiology 461*(6): 645-63.

Ghezzi, C., Murer, H., et al. (2009). "Substrate interactions of the electroneutral Na+-coupled inorganic phosphate cotransporter (NaPi-IIc)." *J Physiol 587*(Pt 17): 4293-307.

Gisler, S. M., Kittanakom, S., et al. (2008). "Monitoring protein-protein interactions between the mammalian integral membrane transporters and PDZ-interacting partners using a modified split-ubiquitin membrane yeast two-hybrid system." *Mol Cell Proteomics 7*(7): 1362-77.

Gonzales, A. L., Lee, W., et al. (2007). "Turnover rate of the gamma-aminobutyric acid transporter GAT1." *J Membr Biol 220*(1-3): 33-51.

Graham, C., Nalbant, P., et al. (2003). "Characterization of a type IIb sodium-phosphate cotransporter from zebrafish (Danio rerio) kidney." *American Journal of Physiology - Renal Physiology 284*(4): F727-36.

Haito-Sugino, S., Ito, M., et al. (2012). "Processing and stability of type IIc sodium-dependent phosphate cotransporter mutations in patients with hereditary hypophosphatemic rickets with hypercalciuria." *Am J Physiol Cell Physiol 302*(9): C1316-30.

Harris, R. M., Webb, D. C., et al. (2001). "Characterization of PitA and PitB from Escherichia coli." *J Bacteriol 183*(17): 5008-14.

Hartmann, C. M., Wagner, C. A., et al. (1995). "Transport characteristics of a murine renal Na/Pi-cotransporter." *Pflugers Archiv. European Journal of Physiology 430*(5): 830-6.

Hediger, M. A., Romero, M. F., et al. (2004). "The ABCs of solute carriers: physiological, pathological and therapeutic implications of human membrane transport proteins. Introduction." *Pflugers Archiv. European Journal of Physiology 447*(5): 465-8.

Hernando, N., Karim-Jimenez, Z., et al. (2001). "Molecular determinants for apical expression and regulatory membrane retrieval of the type IIa Na/P_i cotransporter." *Kidney International 60*(2): 431-5.

Hilfiker, H., Hattenhauer, O., et al. (1998). "Characterization of a murine type II sodium-phosphate cotransporter expressed in mammalian small intestine." *Proceedings of the National Academy of Sciences of the United States of America 95*(24): 14564-9.

Hilgemann, D. W.&Lu, C. C. (1998). "Giant membrane patches: improvements and applications." *Methods Enzymol 293*: 267-80.

Hoffmann, N., Thees, M., et al. (1976). "Phosphate transport by isolated renal brush border vesicles." *Pflugers Arch 362*(2): 147-56.

Jaureguiberry, G., Carpenter, T. O., et al. (2008). "A novel missense mutation in SLC34A3 that causes hereditary hypophosphatemic rickets with hypercalciuria in humans identifies threonine 137 as an important determinant of sodium-phosphate cotransport in NaPi-IIc." *Am J Physiol Renal Physiol 295*(2): F371-9.

Johann, S. V., Gibbons, J. J., et al. (1992). "GLVR1, a receptor for gibbon ape leukemia virus, is homologous to a phosphate permease of Neurospora crassa and is expressed at high levels in the brain and thymus." *J Virol 66*(3): 1635-40.

Johann, S. V., van Zeijl, M., et al. (1993). "Definition of a domain of GLVR1 which is necessary for infection by gibbon ape leukemia virus and which is highly polymorphic between species." *J Virol 67*(11): 6733-6.

Kaback, H. R., Sahin-Toth, M., et al. (2001). "The kamikaze approach to membrane transport." *Nat Rev Mol Cell Biol 2*(8): 610-20.

Kanner, B. I. (2006). "Structure and function of sodium-coupled GABA and glutamate transporters." *Journal of Membrane Biology 213*(2): 89-100.

Karim-Jimenez, Z., Hernando, N., et al. (2000). "A dibasic motif involved in parathyroid hormone-induced down-regulation of the type IIa NaPi cotransporter." *Proceedings of the National Academy of Sciences of the United States of America 97*(23): 12896-901.

Karim-Jimenez, Z., Hernando, N., et al. (2001). "Molecular determinants for apical expression of the renal type IIa Na+/Pi-cotransporter." *Pflugers Archiv. European Journal of Physiology 442*(5): 782-90.

Karlin, A.&Akabas, M. H. (1998). "Substituted-cysteine accessibility method." *Methods in Enzymology 293*: 123-45.

Kavanaugh, M. P.&Kabat, D. (1996). "Identification and characterization of a widely expressed phosphate transporter/retrovirus receptor family." *Kidney International 49*(4): 959-63.

Kavanaugh, M. P., Miller, D. G., et al. (1994). "Cell-surface receptors for gibbon ape leukemia virus and amphotropic murine retrovirus are inducible sodium-dependent phosphate symporters." *Proceedings of the National Academy of Sciences of the United States of America 91*(15): 7071-5.

Ketteler, M.&Giachelli, C. (2006). "Novel insights into vascular calcification." *Kidney International. Supplement*(105): S5-9.

Kohl, B., Herter, P., et al. (1996). "Na-Pi cotransport in flounder: same transport system in kidney and intestine." *Am J Physiol 270*(6 Pt 2): F937-44.

Kohl, B., Wagner, C. A., et al. (1998). "The Na+-phosphate cotransport system (NaPi-II) with a cleaved protein backbone: implications on function and membrane insertion." *J Physiol 508 (Pt 2)*: 341-50.

Kohler, K., Forster, I. C., et al. (2000). "The functional unit of the renal type IIa Na+/Pi cotransporter is a monomer." *Journal of Biological Chemistry 275*(34): 26113-20.

Kohler, K., Forster, I. C., et al. (2002). "Identification of functionally important sites in the first intracellular loop of the NaPi-IIa cotransporter." *American Journal of Physiology 282*(4): F687-96.

Kohler, K., Forster, I. C., et al. (2002). "Transport function of the renal type IIa Na^+/P_i cotransporter is codetermined by residues in two opposing linker regions." *Journal of General Physiology 120*: 693-703.

Kohler, K., Forster, I. C., et al. (2003). "Essential cysteine residues of the type IIa Na^+/P_i cotransporter." *Pflugers Archiv. European Journal of Physiology 446*(2): 203-10.

Lambert, G., Forster, I. C., et al. (1999). "Properties of the mutant Ser-460-Cys implicate this site in a functionally important region of the type IIa Na^+/P_i cotransporter protein." *Journal of General Physiology 114*(5): 637-52.

Lambert, G., Forster, I. C., et al. (2001). "Cysteine mutagenesis reveals novel structure-function features within the predicted third extracellular loop of the type IIa Na^+/P_i cotransporter." *Journal of General Physiology 117*(6): 533-46.

Lambert, G., Traebert, M., et al. (2000). "Cleavage of disulfide bonds leads to inactivation and degradation of the type IIa, but not type IIb sodium phosphate cotransporter expressed in Xenopus laevis oocytes." *Journal of Membrane Biology 176*(2): 143-9.

Lambert, G., Traebert, M., et al. (1999). "Studies on the topology of the renal type II NaPi-cotransporter." *Pflugers Archiv. European Journal of Physiology 437*(6): 972-8.

Lebens, M., Lundquist, P., et al. (2002). "The nptA gene of Vibrio cholerae encodes a functional sodium-dependent phosphate cotransporter homologous to the type II cotransporters of eukaryotes." *Journal of Bacteriology 184*(16): 4466-74.

Loghman-Adham, M. (1996). "Use of phosphonocarboxylic acids as inhibitors of sodium-phosphate cotransport." *General Pharmacology 27*(2): 305-12.

Loo, D. D., Eskandari, S., et al. (2002). A kinetic model for secondary active transport. Membrane Transport and Renal Physiology. H. E. Layton and A. M. Weinstein, Springer**:** 65-84.

Loo, D. D., Hazama, A., et al. (1993). "Relaxation kinetics of the Na^+/glucose cotransporter." *Proceedings of the National Academy of Sciences of the United States of America 90*(12): 5767-71.

Lorenz-Depiereux, B., Benet-Pages, A., et al. (2006). "Hereditary Hypophosphatemic Rickets with Hypercalciuria Is Caused by Mutations in the Sodium-Phosphate Cotransporter Gene SLC34A3." *American Journal of Human Genetics 78*(2): 193-201.

Lundquist, P., Murer, H., et al. (2007). "Type II Na+-Pi cotransporters in osteoblast mineral formation: regulation by inorganic phosphate." *Cell Physiol Biochem 19*(1-4): 43-56.

Madjdpour, C., Bacic, D., et al. (2004). "Segment-specific expression of sodium-phosphate cotransporters NaPi-IIa and -IIc and interacting proteins in mouse renal proximal tubules." *Pflugers Archiv. European Journal of Physiology 448*(4): 402-10.

Magagnin, S., Werner, A., et al. (1993). "Expression cloning of human and rat renal cortex Na/P_i cotransport." *Proceedings of the National Academy of Sciences of the United States of America 90*(13): 5979-83.

Mager, S., Naeve, J., et al. (1993). "Steady states, charge movements, and rates for a cloned GABA transporter expressed in Xenopus oocytes." *Neuron 10*(2): 177-88.

Martinez, P.&Persson, B. L. (1998). "Identification, cloning and characterization of a derepressible Na+-coupled phosphate transporter in Saccharomyces cerevisiae." *Molecular and General Genetics 258*(6): 628-38.

Matsuo, A., Negoro, T., et al. (2005). "Inhibitory effect of JTP-59557, a new triazole derivative, on intestinal phosphate transport in vitro and in vivo." *Eur J Pharmacol 517*(1-2): 111-9.

Meinild, A. K.&Forster, I. C. (2012). "Using lithium to probe sequential cation interactions with GAT1." *Am J Physiol Cell Physiol*.

Miller, D. G.&Miller, A. D. (1994). "A family of retroviruses that utilize related phosphate transporters for cell entry." *J Virol 68*(12): 8270-6.

Miyamoto, K., Haito-Sugino, S., et al. (2011). "Sodium-dependent phosphate cotransporters: lessons from gene knockout and mutation studies." *Journal of Pharmaceutical Sciences 100*(9): 3719-30.

Miyamoto, K., Segawa, H., et al. (2004). "Physiological regulation of renal sodium-dependent phosphate cotransporters." *Japanese Journal of Physiology 54*: 93-102.

Moe, O. W. (2009). "PiT-2 coming out of the pits." *Am J Physiol Renal Physiol 296*(4): F689-90.

Murer, H., Hernando, N., et al. (2000). "Proximal tubular phosphate reabsorption: molecular mechanisms." *Physiological Reviews 80*(4): 1373-409.

Nalbant, P., Boehmer, C., et al. (1999). "Functional characterization of a Na^+-phosphate cotransporter (NaPi-II) from zebrafish and identification of related transcripts." *Journal of Physiology 520 Pt 1*: 79-89.

Nishimura, M.&Naito, S. (2008). "Tissue-specific mRNA expression profiles of human solute carrier transporter superfamilies." *Drug Metab Pharmacokinet 23*(1): 22-44.

O'Hara, B., Johann, S. V., et al. (1990). "Characterization of a human gene conferring sensitivity to infection by gibbon ape leukemia virus." *Cell Growth and Differentiation 1*(3): 119-27.

O'Mara, M., Oakley, A., et al. (2006). "Mechanism and putative structure of B(0)-like neutral amino acid transporters." *Journal of Membrane Biology 213*(2): 111-8.

Olah, Z., Lehel, C., et al. (1994). "The cellular receptor for gibbon ape leukemia virus is a novel high affinity sodium-dependent phosphate transporter." *Journal of Biological Chemistry 269*(41): 25426-31.

Parent, L., Supplisson, S., et al. (1992). "Electrogenic properties of the cloned Na^+/glucose cotransporter: II. A transport model under nonrapid equilibrium conditions.[erratum appears in J Membr Biol 1992 Nov;130(2):203]." *Journal of Membrane Biology 125*(1): 63-79.

Pedersen, L., Johann, S. V., et al. (1995). "Chimeras of receptors for gibbon ape leukemia virus/feline leukemia virus B and amphotropic murine leukemia virus reveal different modes of receptor recognition by retrovirus." *J Virol 69*(4): 2401-5.

Pedersen, L., van Zeijl, M., et al. (1997). "Fungal phosphate transporter serves as a receptor backbone for gibbon ape leukemia virus." *J Virol 71*(10): 7619-22.

Picard, N., Capuano, P., et al. (2010). "Acute parathyroid hormone differentially regulates renal brush border membrane phosphate cotransporters." *Pflugers Archiv. European Journal of Physiology 460*(3): 677-87.

Radanovic, T., Gisler, S. M., et al. (2006). "Topology of the type IIa Na+/P(i) cotransporter." *Journal of Membrane Biology 212*(1): 41-9.

Ravera, S., Virkki, L. V., et al. (2007). "Deciphering PiT transport kinetics and substrate specificity using electrophysiology and flux measurements." *Am J Physiol Cell Physiol 293*(2): C606-20.

Reimer, R. J.&Edwards, R. H. (2004). "Organic anion transport is the primary function of the SLC17/type I phosphate transporter family." *Pflugers Arch 447*(5): 629-35.

Sacher, A., Nelson, N., et al. (2002). "Presteady-state and steady-state kinetics and turnover rate of the mouse gamma-aminobutyric acid transporter (mGAT3)." *Journal of Membrane Biology 190*(1): 57-73.

Salaun, C., Marechal, V., et al. (2004). "Transport-deficient Pit2 phosphate transporters still modify cell surface oligomers structure in response to inorganic phosphate." *J Mol Biol 340*(1): 39-47.

Salaun, C., Rodrigues, P., et al. (2001). "Transmembrane topology of PiT-2, a phosphate transporter-retrovirus receptor." *J Virol 75*(12): 5584-92.

Saliba, K. J., Martin, R. E., et al. (2006). "Sodium-dependent uptake of inorganic phosphate by the intracellular malaria parasite." *Nature 443*(7111): 582-5.

Schaffhauser, D. F., Patti, M., et al. (2012). "An integrated field-effect microdevice for monitoring membrane transport in Xenopus laevis oocytes via lateral proton diffusion." *PLoS One*.

Screpanti, E.&Hunte, C. (2007). "Discontinuous membrane helices in transport proteins and their correlation with function." *Journal of Structural Biology 159*(2): 261-7.

Segawa, H., Kaneko, I., et al. (2002). "Growth-related renal type II Na/Pi cotransporter." *Journal of Biological Chemistry 277*(22): 19665-72.

Tatsumi, S., Segawa, H., et al. (1998). "Molecular cloning and hormonal regulation of PiT-1, a sodium-dependent phosphate cotransporter from rat parathyroid glands." *Endocrinology 139*(4): 1692-9.

Tenenhouse, H. S. (2005). "Regulation of phosphorus homeostasis by the type IIa Na/phosphate cotransporter " *Annual Review of Nutrition 25*: 197-214.

Tenenhouse, H. S.&Murer, H. (2003). "Disorders of renal tubular phosphate transport." *Journal of the American Society of Nephrology 14*(1): 240-8.

Uckert, W., Willimsky, G., et al. (1998). "RNA levels of human retrovirus receptors Pit1 and Pit2 do not correlate with infectibility by three retroviral vector pseudotypes." *Human Gene Therapy 9*(17): 2619-27.

van Veen, H. W. (1997). "Phosphate transport in prokaryotes: molecules, mediators and mechanisms." *Antonie Van Leeuwenhoek 72*(4): 299-315.

van Zeijl, M., Johann, S. V., et al. (1994). "A human amphotropic retrovirus receptor is a second member of the gibbon ape leukemia virus receptor family." *Proc Natl Acad Sci U S A 91*(3): 1168-72.

Versaw, W. K.&Metzenberg, R. L. (1995). "Repressible cation-phosphate symporters in Neurospora crassa." *Proc Natl Acad Sci U S A 92*(9): 3884-7.

Villa-Bellosta, R., Bogaert, Y. E., et al. (2007). "Characterization of phosphate transport in rat vascular smooth muscle cells. Implications for vascular calcification." *Arterioscler Thromb Vasc Biol*.

Villa-Bellosta, R., Bogaert, Y., Levi, M., Sorribas, V. (2007). Toxicity of phosphonoformic acid in vascular smooth muscle cells:relationship to vascular calcification. FASEB.

Villa-Bellosta, R., Ravera, S., et al. (2009). "The Na+-Pi cotransporter PiT-2 (SLC20A2) is expressed in the apical membrane of rat renal proximal tubules and regulated by dietary Pi." *Am J Physiol Renal Physiol 296*(4): F691-9.

Villa-Bellosta, R.&Sorribas, V. (2008). "Role of rat sodium/phosphate cotransporters in the cell membrane transport of arsenate." *Toxicology and Applied Pharmacology 232*(1): 125-34.

Villa-Bellosta, R.&Sorribas, V. (2008). "Role of rat sodium/phosphate cotransporters in the cell membrane transport of arsenate." *Toxicol Appl Pharmacol 232*(1): 125-34.

Villa-Bellosta, R.&Sorribas, V. (2009). "Different effects of arsenate and phosphonoformate on P(i) transport adaptation in opossum kidney cells." *Am J Physiol Cell Physiol 297*(3): C516-25.

Villa-Bellosta, R.&Sorribas, V. (2010). "Arsenate transport by sodium/phosphate cotransporter type IIb." *Toxicology and Applied Pharmacology 247*(1): 36-40.

Virkki, L. V., Biber, J., et al. (2007). "Phosphate transporters: a tale of two solute carrier families." *Am J Physiol Renal Physiol 293*(3): F643-54.

Virkki, L. V., Forster, I. C., et al. (2005). "Functionally important residues in the predicted 3rd transmembrane domain of the type IIa sodium-phosphate co-transporter (NaPi-IIa)." *Journal of Membrane Biology 206*(3): 227-38.

Virkki, L. V., Forster, I. C., et al. (2005). "Substrate interactions in the human type IIa sodium-phosphate cotransporter (NaPi-IIa)." *American Journal of Physiology 288*: F969-F981.

Virkki, L. V., Murer, H., et al. (2006). "Mapping conformational changes of the type IIb Na^+/P_i cotransporter by voltage clamp fluorometry." *Journal of Biological Chemistry 281*: 28837-28849.

Virkki, L. V., Murer, H., et al. (2006). "Voltage clamp fluorometric measurements on a type II Na^+-coupled P_i cotransporter: shedding light on substrate binding order." *Journal of General Physiology 127*: 539-555.

Wadiche, J. I., Arriza, J. L., et al. (1995). "Kinetics of a human glutamate transporter." *Neuron 14*(5): 1019-27.

Wallin, A.&Ryrfeldt, A. (1995). "The toxicity of Foscarnet (phosphonoformic acid, trisodium salt; PFA) studied in cultured dog renal Tubular Cells." *Toxicol In Vitro 9*(3): 237-44.

Wang, C., Li, Y., et al. (2012). "Mutations in SLC20A2 link familial idiopathic basal ganglia calcification with phosphate homeostasis." *Nature Genetics 44*(3): 254-6.

Weinstock, J. (2004). "Inhibitors of sodium-dependent phosphate transport." *Expert Opinion Therapeutic Patents 14*(1): 3.

Weiss, J. N. (1997). "The Hill equation revisited: uses and misuses." *FASEB Journal 11*(11): 835-41.

Werner, A.&Kinne, R. K. (2001). "Evolution of the Na-P_i cotransport systems." *American Journal of Physiology 280*(2): R301-12.

Werner, A., Moore, M. L., et al. (1991). "Cloning and expression of cDNA for a Na/Pi cotransport system of kidney cortex." *Proc Natl Acad Sci U S A 88*(21): 9608-12.

Werner, A., Murer, H., et al. (1994). "Cloning and expression of a renal Na-Pi cotransport system from flounder." *Am J Physiol 267*(2 Pt 2): F311-7.

Yamashita, A., Singh, S. K., et al. (2005). "Crystal structure of a bacterial homologue of Na+/Cl--dependent neurotransmitter transporters." *Nature 437*(7056): 215-23.

Zampighi, G. A., Kreman, M., et al. (1995). "A method for determining the unitary functional capacity of cloned channels and transporters expressed in Xenopus laevis oocytes." *Journal of Membrane Biology 148*(1): 65-78.

Figure 1

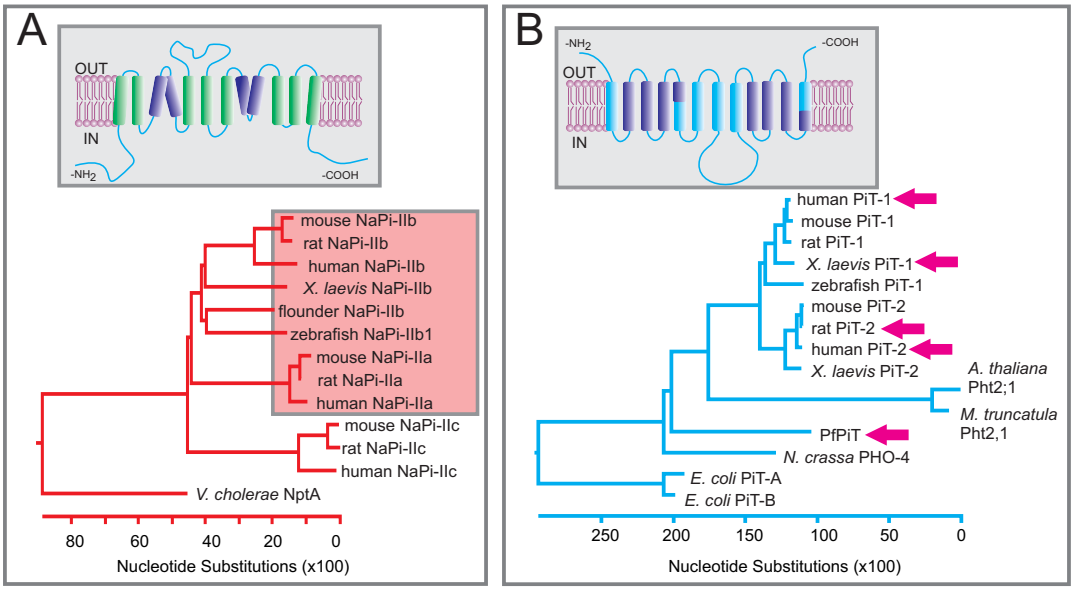
A
OUT
IN
-NH2
-COOH
mouse NaPi-IIb
rat NaPi-IIb
human NaPi-IIb
X. laevis NaPi-IIb
flounder NaPi-IIb
zebrafish NaPi-IIb1
mouse NaPi-IIa
rat NaPi-IIa
human NaPi-IIa
mouse NaPi-IIc
rat NaPi-IIc
human NaPi-IIc
V. cholerae NptA
80
60
40
20
0
Nucleotide Substitutions (x100)
B
-NH2
-COOH
OUT
IN
human PiT-1
mouse PiT-1
rat PiT-1
X. laevis PiT-1
zebrafish PiT-1
mouse PiT-2
rat PiT-2
human PiT-2
X. laevis PiT-2
A. thaliana Pht2;1
M. truncatula Pht2,1
PfPiT
N. crassa PHO-4
E. coli PiT-A
E. coli PiT-B
250
200
150
100
50
0
Nucleotide Substitutions (x100)

Figure 2

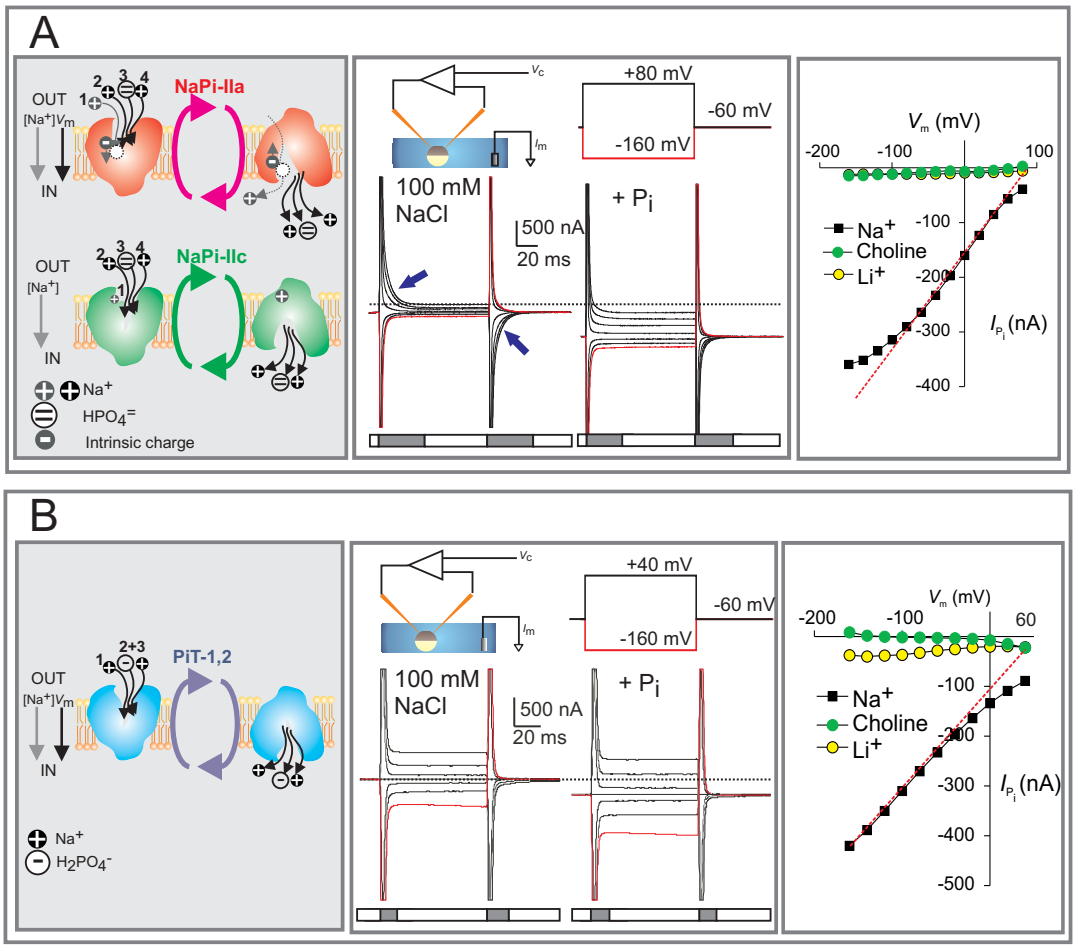
A
OUT
[Na+]Vm
IN
NaPi-IIa
OUT
[Na+]
IN
NaPi-IIc
Na+
HPO4=
Intrinsic charge
Vc
Im
+80 mV
-60 mV
-160 mV
100 mM
NaCl
500 nA
20 ms
+ Pi
Vm (mV)
-200
-100
100
Na+
Choline
Li+
-100
-200
-300
-400
IPi (nA)
B
OUT
[Na+]Vm
IN
2+3
PiT-1,2
Na+
H2PO4-
Vc
Im
+40 mV
-60 mV
-160 mV
100 mM
NaCl
500 nA
20 ms
+ Pi
Vm (mV)
-200
-100
60
Na+
Choline
Li+
-100
-200
-300
-400
-500
IPi (nA)

Figure 3

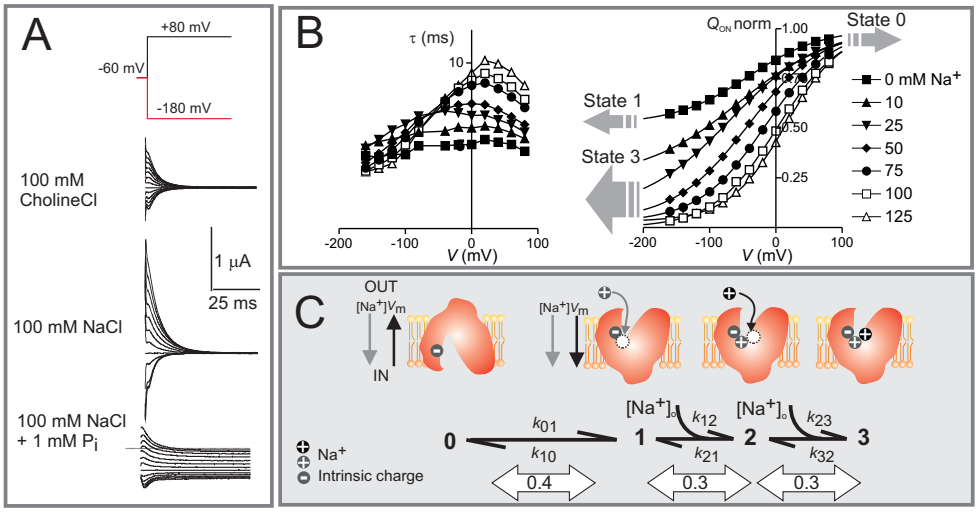
A
+80 mV
-60 mV
-180 mV
100 mM CholineCl
1 µA
25 ms
100 mM NaCl
100 mM NaCl + 1 mM Pi
B
τ (ms)
10
-200
-100
0
100
V (mV)
Q_ON norm
1.00
0.50
0.25
State 0
State 1
State 3
0 mM Na+
10
25
50
75
100
125
C
OUT
[Na+]Vm
IN
[Na+]o
[Na+]o
0
1
2
3
k01
k10
k12
k21
k23
k32
0.4
0.3
0.3
Na+
Intrinsic charge

Figure 4

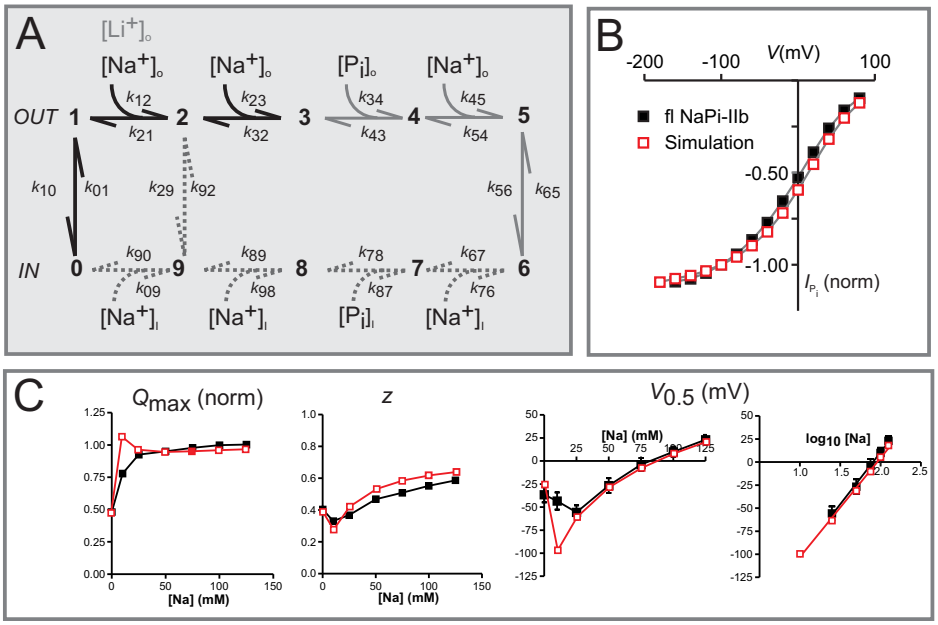
A
[Li+]o
[Na+]o
[Na+]o
[Pi]o
[Na+]o
OUT
1
2
3
4
5
k12
k21
k23
k32
k34
k43
k45
k54
k10
k01
k29
k92
k56
k65
IN
0
9
8
7
6
k90
k09
k89
k98
k78
k87
k67
k76
[Na+]i
[Na+]i
[Pi]i
[Na+]i
B
-200
-100
V(mV)
100
fl NaPi-IIb
Simulation
-0.50
-1.00
IPi (norm)
C
Qmax (norm)
z
V0.5 (mV)
[Na] (mM)
[Na] (mM)
[Na] (mM)
log10 [Na]

Figure 5

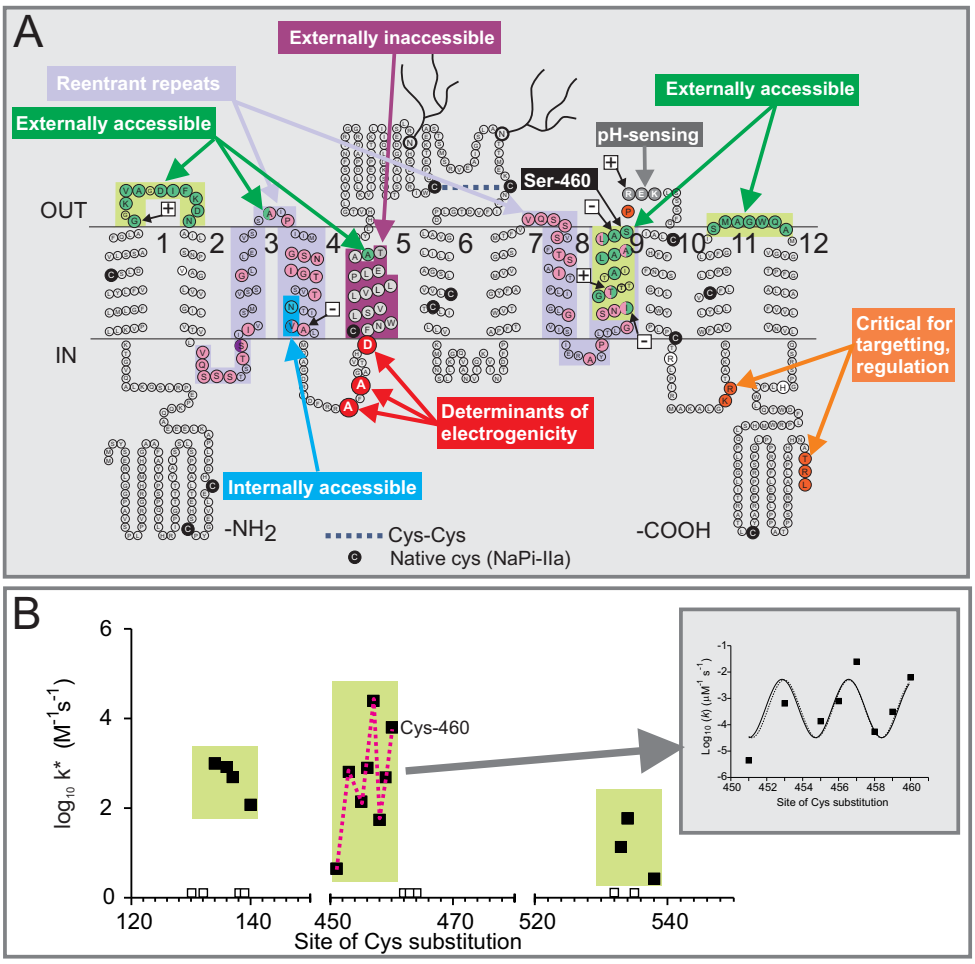
A
Externally inaccessible
Reentrant repeats
Externally accessible
Externally accessible
pH-sensing
Ser-460
OUT
IN
1 2 3 4 5 6 7 8 9 10 11 12
Critical for targetting, regulation
Determinants of electrogenicity
Internally accessible
-NH2
-COOH
Cys-Cys
Native cys (NaPi-IIa)
B
log10 k* (M-1s-1)
Cys-460
Site of Cys substitution
Site of Cys substitution

Figure 6

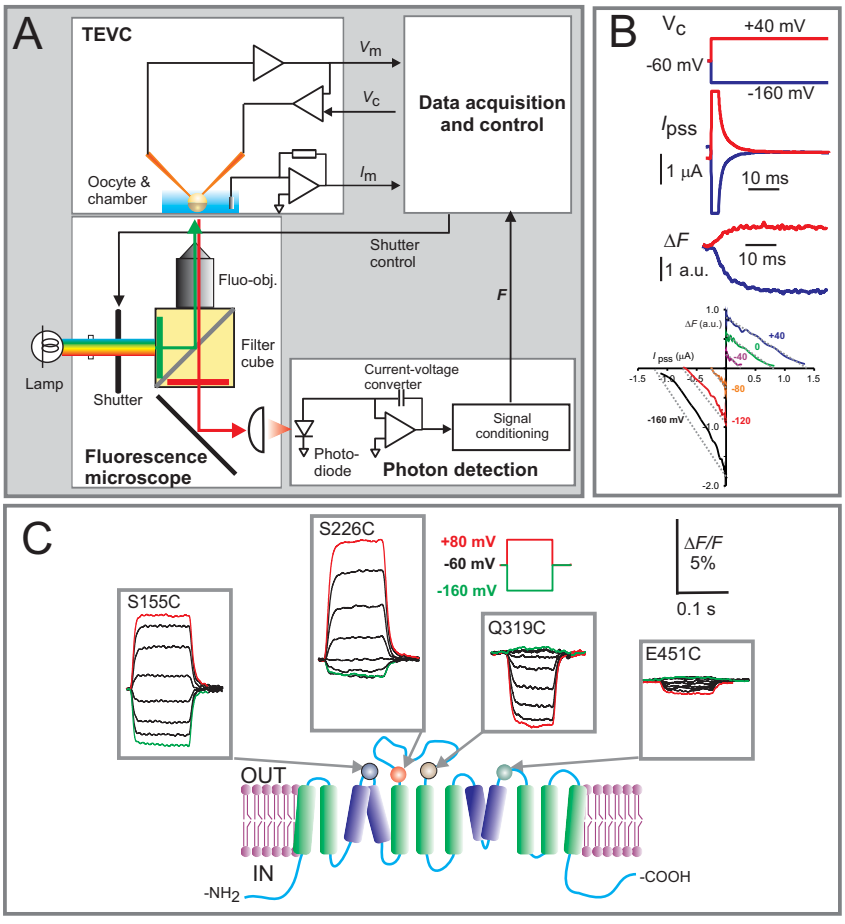
A
TEVC
V_m
V_c
I_m
Oocyte & chamber
Data acquisition and control
Shutter control
F
Fluo-obj.
Filter cube
Lamp
Shutter
Fluorescence microscope
Current-voltage converter
Signal conditioning
Photo-diode
Photon detection
B
V_c
+40 mV
-60 mV
-160 mV
I_{pss}
1 µA
10 ms
ΔF
1 a.u.
10 ms
C
S226C
+80 mV
-60 mV
-160 mV
ΔF/F
5%
0.1 s
S155C
Q319C
E451C
OUT
IN
$-NH_2$
-COOH

Figure 7

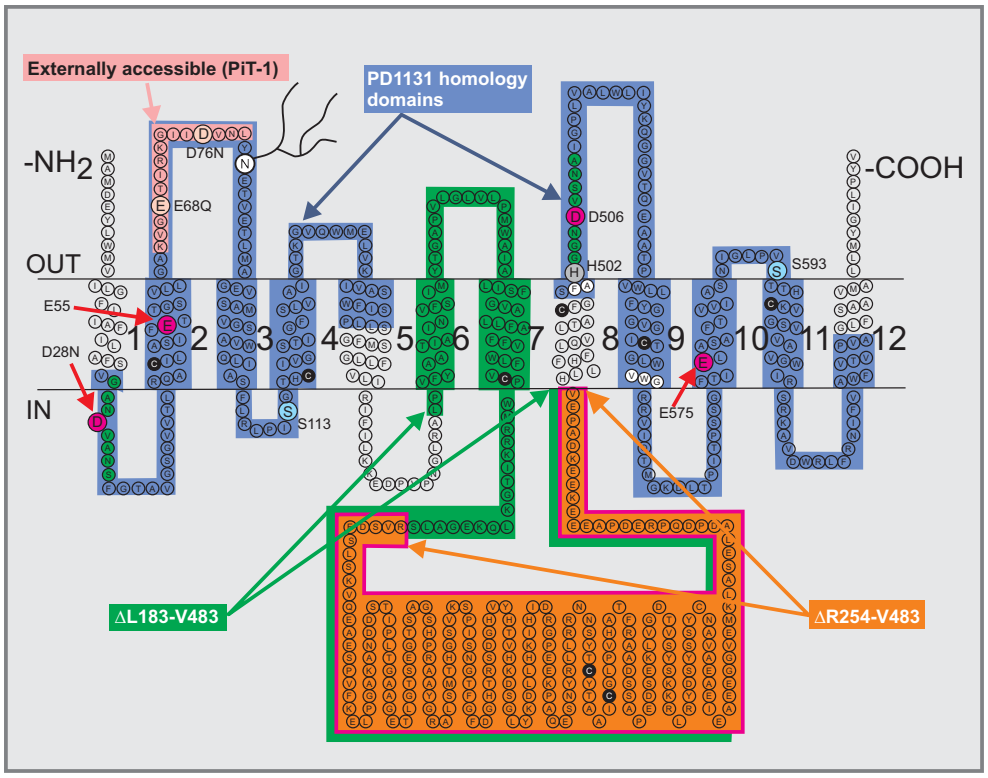
Externally accessible (PiT-1)
PD1131 homology domains
-NH2
-COOH
OUT
IN
D76N
E68Q
D506
H502
S593
E55
D28N
S113
E575
1
2
3
4
5
6
7
8
9
10
11
12
ΔL183-V483
ΔR254-V483